University of Alberta Library
0 1620 3644038 4

Digitized by the Internet Archive
in 2021 with funding from
University of Alberta Libraries

https://archive.org/details/Wright2005

University of Alberta

Library Release Form

Name of Author [illegible]

Title of Thesis [illegible]

Degree [illegible]

Year this Degree Granted [illegible]

[illegible]

[illegible]

[illegible]

University of Alberta

Library Release Form

Name of Author:	Robert W. Wright
Title of Project:	Effect of Heat Input and FCAW Wire Size on Charpy V-Notch Test Results
Degree:	Master of Engineering in Welding Engineering
Year this Degree Granted:	2005

Permission is hereby granted to the University of Alberta Library to reproduce single copies of this thesis and to lend or sell such copies for private, scholarly or scientific research purposes only.

The author reserves all other publication and other rights in association with the copyright in the thesis, and except as herein before provided, neither the thesis nor any substantial portion thereof may be printed or otherwise reproduced in any material form whatsoever without the author's prior written permission.

Signature

10523 – 140 Street
Edmonton, Alberta
T5N 2M1

University of Alberta

Effect of Heat Input and FCAW Wire Size on Charpy V-Notch Test Results

by

Robert W. Wright

A project submitted to the Faculty of Chemical and Materials Engineering
in partial fulfillment of the requirements for the degree of
Master of Engineering

in

Welding Engineering

Department of Chemical and Materials Engineering

Edmonton, Alberta

Spring 2005

UNIVERSITY LIBRARY

University of Alberta

Faculty of Chemical & Materials Engineering

The undersigned certify that they have read, and recommend to the Faculty of Chemical & Materials Engineering for acceptance, a project entitled Effect of Heat Input and FCAW Wire Size on Charpy V-Notch Test Results submitted by Robert W. Wright in partial fulfillment of the requirements for the degree of Master of Engineering in Welding Engineering.

B.M. Patchett, P.Eng., Ph.D.

Abstract

It is well known that an increase in heat input results in a decrease in weld metal toughness for single pass welds in ferritic structural steels. The effect of multiple weld passes, however, creates a much more complex microstructural system in which the resulting toughness is not easy to predict when heat inputs vary. To assess such effects, the flux core arc welding process was used to deposit multipass welds at 3 different heat inputs. It is seen that increasing the heat input does not always have a detrimental effect on the Charpy V-notch toughness values of weld metal in multipass welds and that varying the electrode size results in different toughness values at the same heat input. These differences are due, in part, to notch location within the resulting microstructure and the amount of reaustenitized, annealed, and tempered weld metal created from depositing subsequent weld passes.

ACKNOWLEDGEMENTS

This research was made possible with the assistance of two companies; Waiward Steel Fabricators for the supply of material, manpower and consumables and Ludwig & Associates Engineering for the completion of all material testing.

Table of Contents

1.0 **Introduction** 1

2.0 **Background Information** 2

- 2.1 Welding 2
  - 2.1.1 The Welding Arc 2
  - 2.1.2 Welding Processes 2
  - 2.1.3 Flux Core Arc Welding 3
  - 2.1.4 Welding Wire Properties 4
  - 2.1.5 Heat Input 5
- 2.2 Metallurgy 7
  - 2.2.1 Weld Metal Solidification 7
  - 2.2.2 Solid State Transformations in the Weld Metal 9
  - 2.2.3 Alloying Elements 11
  - 2.2.4 Effects of Shielding Gas 13
  - 2.2.5 The Heat Affected Zone 15
- 2.3 Fracture 16
  - 2.3.1 Fracture Toughness 17
  - 2.3.2 Charpy V-Notch Impact Test 21
  - 2.3.3 Application of Charpy V-Notch Test Results 24

3.0 **Materials and Experimental Procedures** 25

- 3.1 Welding Equipment 25
- 3.2 Welding Consumables 25
- 3.3 Base Metal 26
- 3.4 Welding Data 26
- 3.5 Charpy V-Notch Testing 26
- 3.6 Metallography 26

4.0 **Results and Discussion** 27

5.0 **Conclusions** 30

6.0 **Future Work** 32

7.0 **References** 33

8.0 **Appendices** 37

List of Tables

Table 1: AWS A5.20-95 weld metal chemical composition requirements in maximum weight percent for multipass welds made with an EXT-1(M), E7XT-5(M) and E7XT-9(M)

Table B1: Welding Data

Table C1: CVN Impact Data (Joules)

Table E1: Hardness testing results – Vickers test, 10 Kg load

List of Figures

Figure 1: Flux Core Arc Welding

Figure 2: Penetration patterns based on shielding gas composition

Figure 3: AWS A5.20 Classification System

Figure 4: AWS A5.29 Classification System

Figure 5: Current carrying area of a tubular wire vs. solid wire

Figure 6: Schematic illustration showing effect of welding speed on dendritic growth

Figure 7: Schematic of weld CCT diagram showing selected microstructures

Figure 8: Shielding gas effect on Charpy V-notch impact toughness

Figure 9: Weld metal with heat affected zone

Figure 10: Normal distribution for Charpy V-notch impact energies of CSA G40.21, Grade 350WT Cat 4 plate

Figure 11: Stress components ahead of a crack

Figure 12: Crack Tip Loading Modes

Figure 13: Crack opening displacement test and inferred CTOD

Figure 14: Charpy V-notch general testing configuration

Figure 15: Typical Charpy V-notch test behavior for structural steels

Figure 16: Effect of strain rate on Charpy V-notch impact data

Figure C1: Charpy V-notch specimen location

Figure C2: CVN Impact Values for 1.6mm Welding Wire

Figure C3: CVN Impact Values for 2.4mm Welding Wire

Figure D1: Specimen 5, Macrostructure, 2% Nital Etch

Figure D2: Specimen 5, Weld Metal Microstructure, 2% Nital Etch, 400x Magnification

Figure D3: Specimen 5, Untempered Weld Metal, Picral Etch, 400x Magnification

Figure D4: Specimen 5, Weld Metal Reheat Zone, Picral Etch, 400x Magnification

Figure D5: Specimen 6, Macrostructure, 2% Nital Etch

Figure D6: Specimen 6, Weld Metal Microstructure, 2% Nital Etch, 400x Magnification

Figure D7: Specimen 6, Untempered Weld Metal, Picral Etch, 400x Magnification

Figure D8: Specimen 6, Weld Metal Reheat Zone, Picral Etch, 400x Magnification

Figure D9: Specimen 7, Macrostructure, 2% Nital Etch

Figure D10: Specimen 7, Weld Metal Microstructure, 2% Nital Etch, 400x Magnification

Figure D11: Specimen 7, Untempered Weld Metal, Picral Etch, 400x Magnification

Figure D12: Specimen 7, Weld Metal Reheat Zone, Picral Etch, 400x Magnification

Figure D13: Specimen 10, Macrostructure, 2% Nital Etch

Figure D14: Specimen 10, Weld Metal Microstructure, 2% Nital Etch, 400x Magnification

Figure D15: Specimen 10, Untempered Weld Metal, Picral Etch, 400x Magnification

Figure D16: Specimen 10, Weld Metal Reheat Zone, Picral Etch, 400x Magnification

Figure F1: Specimen 5, HAZ Microstructure, 2% Nital Etch, 400X Magnification

Figure F2: Specimen 6, HAZ Microstructure, 2% Nital Etch, 400X Magnification

Figure F3: Specimen 7, HAZ Microstructure, 2% Nital Etch, 400X Magnification

Figure F4: Specimen 10, HAZ Microstructure, 2% Nital Etch, 400X Magnification

List of Symbols

A	area
a	crack length
σ	stress
τ	shear stress
K	fracture toughness
r	radius
K_I	fracture toughness, mode I loading
B	Material thickness for which K_{mat} is required
β	geometric factor
a	crack length
ε	strain
ε_{el}	elastic strain
ε_{pl}	plastic strain
E	modulus of elasticity
F	dimensionless parameter determined from tensile testing
n	strain-hardening parameter
J	material energy release rate
H	geometry factor
K_{IC}	plane-strain fracture toughness
K_{ID}	dynamic impact plane strain
T	temperature
K_{mat}	material toughness determined by Charpy V-notch data

1.0 INTRODUCTION

Since its inception, the state of arc welding has evolved substantially. Understanding the fundamental characteristics of the welding arc, the manner in which the weld metal is transferred across the arc, and weld metal solidification has created a need for improved machinery and filler metal manufacturing methods to provide products in which weld metal deposition rate is increased and mechanical properties are optimized. Advances in materials science have allowed the designers of welding filler metals to more accurately predict the resulting weld metal properties from the alloying elements used and shielding medium specified.

Despite these advances, many of the resulting weld metal properties are controlled by the welder and the parameters specified by the welding engineer to deposit the weld metal. Codes and standards have been created in an attempt to control the varying weld metal properties that can be produced. More specifically, these codes or standards specify testing requirements that must produce minimum values depending on the classification of the materials being joined. Certain welding parameters, as defined by the governing code or standard, must be controlled depending on the required mechanical properties. As the engineering community becomes more knowledgeable about the detrimental effects of varying properties, the testing requirements and quality assurance provisions are increasing. In the last few years, the requirement for Charpy V-notch impact testing has become more widespread as many failures seen in service can be accounted for due to a materials susceptibility to brittle failure. It is seen, however, that the reliance on the applicability of the information provided from the standard Charpy V-notch test is not always well placed.

The following sections present many of the factors that contribute to the material toughness of a weldment as well as the theory behind crack growth and the information provided from the Charpy V-notch test. Testing has been performed on multipass welds created by the flux cored arc welding process to create an engineering data base. The effects of heat input as well as filler metal diameter have been evaluated to determine their relationship to the toughness of a weld metal when tested with the Charpy V-notch test.

2.0 BACKGROUND INFORMATION

2.1 Welding

2.1.1 The Welding Arc

Broadly stated, arc welding is the joining of metals by a fusion process involving an electrical discharge that is carried through a conducting plasma at high currents and low voltages. This can be accomplished by melting the existing base metals to form a solid bond between the two pieces or by adding filler metal where an electrode is melted and transferred across the arc and into the joint. The arc forms in a columnar pattern in which the gas is thermally ionized and the current is carried by the electrons and ions.[1] Using a direct current, electrode positive process, electrons are emitted from the cathode (the base metal) and accelerated by the arc voltage until they collide with the anode, thereby creating heat. The positive ions travel in the opposite direction and heat the base metal by striking it. The motion of the electrons, ions, and atoms is greatest at the central region of the plasma stream where it is the hottest and is reduced as the edge of the arc is approached.[2] Changing the shielding media can change the thermal gradient between the electrode and base metal and changing the arc length or in some cases adjusting the current available can also vary the heat distribution. The resulting weld metal composition and mechanical properties are dependant on the reactions that occur within the welding arc and also in the weld pool.

2.1.2 Welding Processes

Industry is constantly searching for ways to speed up the time required to join metals including the speed of the actual welding process as well as an increase in the proportion of time that the welding arc is actually engaged. Shielded metal arc welding (SMAW) is one of the oldest methods of arc welding. It involves using a welding rod that is covered with a coating that provides shielding from the atmosphere when melted. While this process has many benefits, including ease of use and mobility, the actual time spent welding is decreased as the majority of SMAW electrodes in use are 14 inches long, requiring the welder to constantly spend time discarding the end of one electrode and preparing another for use. Because of this inefficiency, an improved process, gas metal arc welding (GMAW) was introduced and rapidly gained support from the welding industry. Since the weld properties are very dependant on the wire used, this process is still relatively expensive due to the number of different runs and different alloys that the electrode manufacturer must use to obtain the properties required. Submerged arc welding,

which also generally involves using a solid electrode also gained popularity due to the high arc-on-time and process efficiency. In this process a granular flux is used to provide shielding and can be interchanged to impart different properties in the weld metal. The problem with SAW is the inability to weld in positions other than flat and horizontal fillets as well as the large set-up time making it impractical to weld shorter joints with this process. Flux core arc welding, or "FCAW", was the next process to gain in popularity allowing the electrode manufacturers to put fluxing agents inside of a wire sheath that is also able to be fed continuously thus increasing production. FCAW will be investigated in this paper specifically dealing with the effects of changing the wire size and heat input on the toughness of the weld metal.

2.1.3 Flux Core Arc Welding

As its name implies, flux-cored electrodes consist of a metal sheath with a fluxing agent contained in the core of the consumable. This fluxing agent aids in shielding the molten metal from detrimental atmospheric elements (primarily oxygen and nitrogen), contains alloying elements that improve the mechanical properties of the weldment, and helps create a stable arc. The manufacturing technique for this type of welding consumable involves forming a strip of metal into a "U" shape in order to receive the flux material and then closing the wire by running through a set of forming rolls. Technological advancements have allowed for precise measurements when adding the flux thus avoiding locations within the wire where insufficient amounts of flux may exist creating quality problems in the weld metal. The wire is then passed through a number of drawing dies that stretch the metal and progressively reduces it to the intended electrode diameter. Many manufacturers complete the fabrication process by baking the electrode to remove any detrimental contaminants that may have been picked up during fabrication and also to soften the wire allowing for easier feeding by the welding equipment.

The flux-cored electrode is generally provided in 30 – 60 lb rolls allowing for a continuous feeding of the consumable. This has been seen in industry to greatly increase the amount of time that a welder can spend actually welding. The equipment required for operation involves a constant voltage power source and a wire feeder. The wire used may be one in which a gas shielding must be applied (dual shield) or one that is considered a self-shielding electrode. In this paper, only the dual shielded process will be discussed. The welding parameters that are controlled through the equipment consist of the wire speed (current), the voltage, and the gas flow rate. Welding procedures are created in order to allow for the correct selection of welding parameters that will produce the mechanical properties required for the specific application.

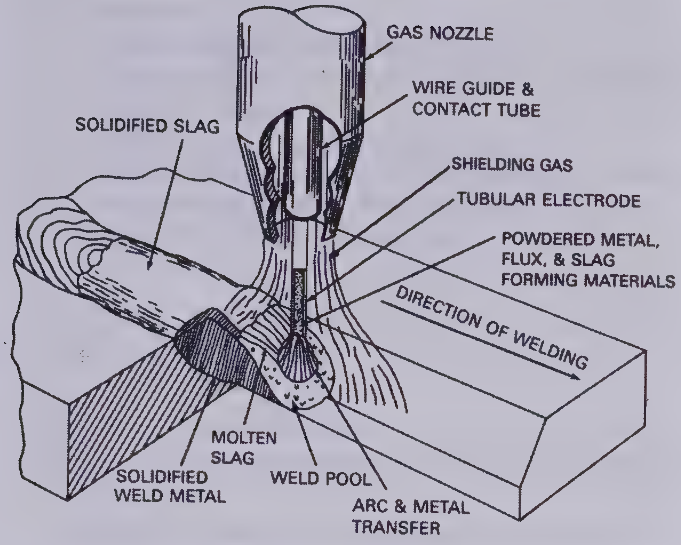

Figure 1: Flux Core Arc Welding[3]

The shielding gas used for FCAW is usually blended argon / carbon dioxide gas, or 100% carbon dioxide. The blended gases are more expensive as the amount of argon is increased but provide a smoother arc and a better bead appearance with no flux left on the weld to be cleaned off. The penetration of the Ar/CO_2 gas is narrower at the base and is not as deep as with 100% CO_2 shielding gas as can be seen in Figure 2.[4] The shielding gas composition has a profound effect on the weld metal chemical composition and microstructure. This will be discussed later.

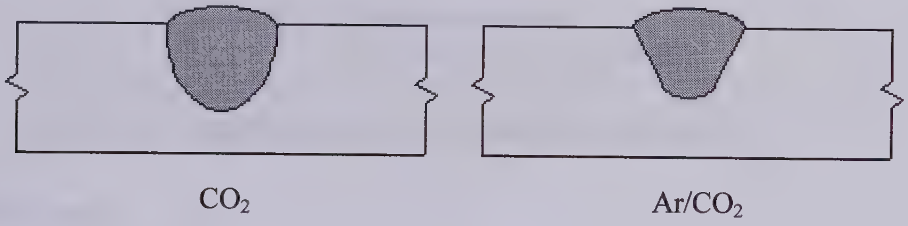

Figure 2: Penetration patterns based on shielding gas composition

2.1.4 Welding Wire Properties

Various specifications contain a classification system for identifying the typical properties that will result from using a specific electrode. AWS Specification A5.20, Carbon Steel Electrodes for Flux Cored Arc Welding and AWS A5.29, Specification for Low-Alloy Steel Electrodes for Flux Cored Arc Welding are internationally recognized specifications that use a letter-number designation for identifying mechanical properties, weld metal chemistry, and required welding conditions such as polarity, shielding gas, and welding positions.

[illegible]

[illegible]

[illegible]

[illegible]

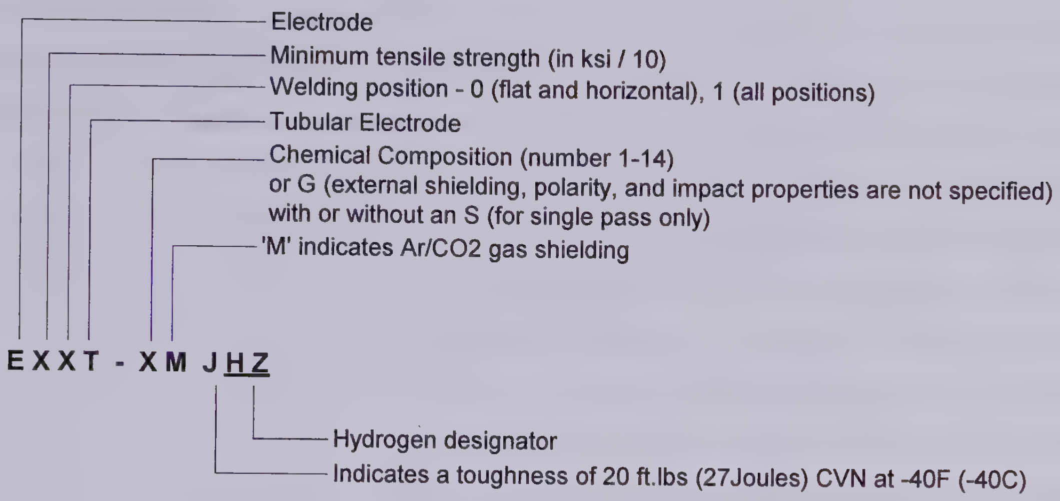
Electrode
Minimum tensile strength (in ksi / 10)
Welding position - 0 (flat and horizontal), 1 (all positions)
Tubular Electrode
Chemical Composition (number 1-14)
or G (external shielding, polarity, and impact properties are not specified)
with or without an S (for single pass only)
'M' indicates Ar/CO2 gas shielding
EXXT - XM JHZ
Hydrogen designator
Indicates a toughness of 20 ft.lbs (27Joules) CVN at -40F (-40C)

Figure 3: AWS A5.20 Classification System[5]

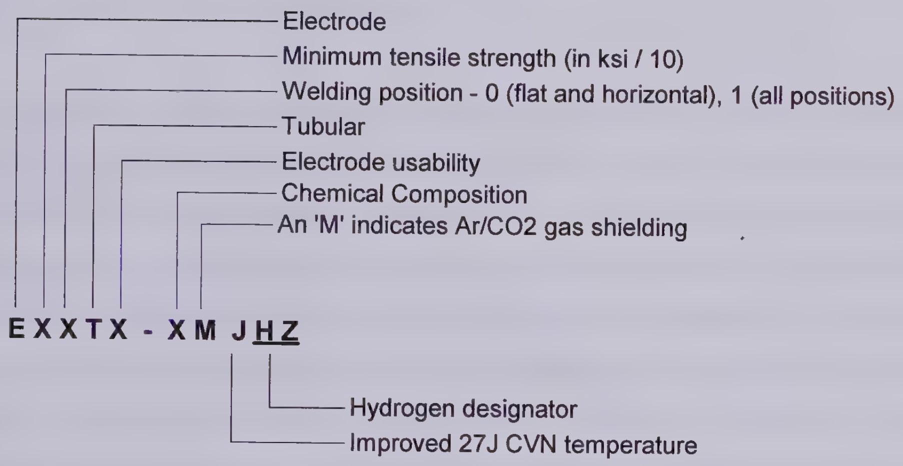
Electrode
Minimum tensile strength (in ksi / 10)
Welding position - 0 (flat and horizontal), 1 (all positions)
Tubular
Electrode usability
Chemical Composition
An 'M' indicates Ar/CO2 gas shielding
EXXTX - XM JHZ
Hydrogen designator
Improved 27J CVN temperature

Figure 4: AWS A5.29 Classification system[6]

2.1.5 Heat Input

The heat input of welding has been well documented and is found to be a function of the current, voltage, and arc travel speed. While the energy transfer obtained from the following equation suggests that no heat is lost to the surroundings, the ability to effectively determine exactly how much of the energy is lost is difficult to determine and has, therefore, not been included in the standard heat input calculation.[8]

$$\text{Heat Input} = \frac{\text{Current} \times \text{Voltage}}{\text{Travel Speed}}$$

The resulting heat input is written in J/mm where the current is measured in amperes (A), voltage in volts (V), and travel speed in millimeters/second. Varying the heat input affects the maximum temperature reached and the cooling rate of the weld zone, which has a profound effect on the microstructure of the weld metal and heat affected zone. If the heat input is high, sufficient amounts of grain coarsening will be experienced both in the weld metal and heat affected zone. If the heat input is too low, fusion defects may occur and heat loss may be fast enough to effectively quench the weld metal creating a hard, brittle microstructure. To increase welding production companies maximize the heat input, allowing a faster rate of weld metal deposition, to a point where corresponding problems in the resulting weld zone are minimized. The size and type of electrode also has a limiting factor on the amount of current that can flow and increased diameters will commonly be used to allow for greater levels of weld metal deposition. Using larger diameter electrodes or solid electrodes versus tubular electrodes, however, do not always provide the productivity gains that are believed to occur.

While it would seem probable that a solid wire used in gas metal arc welding should have higher deposition rates than that of the tubular wire used in flux cored arc welding, the opposite is proven true due to the current density of the electrode. If the same amount of current is used when welding with two different consumable configurations, the area in which the current is allowed to travel is the controlling factor in the melting rate of the electrode. As shown in Figure 5, the area in which the current is able to flow is much greater for a solid electrode than it is for a tubular wire. This decrease in current density causes a reduction in the burn off rate of the electrode, thus decreasing the amount of weld metal deposited at the same heat input. This is also true when changing the size of electrode to be used for welding. If the current is kept the same, a smaller size wire will deposit more weld metal at the same heat input due to the smaller area in which the current flows. The limiting factor is the current carrying capacity that a specific welding electrode size can withstand. As the current density increases, the usability of the electrode will become much more dependant on the inter-relation between the different welding parameters. There will come a point where the electrode will not be able to handle further increases in current and the user will need to increase the area through which the current can flow, thus decreasing the current density.

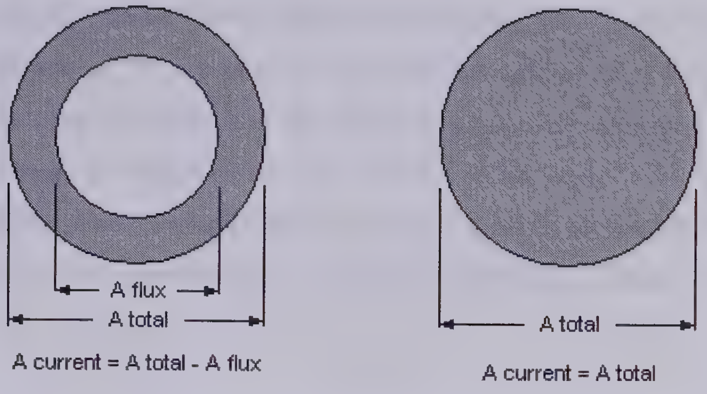

Fig. 5: Current carrying area of a tubular wire vs. solid wire

2.2 Metallurgy

While the fundamentals of physical metallurgy are well defined for the relatively simplistic heat treatments used to manufacture steel, the act of welding, in which a large amount of heat is put into the joint in a very short time, is much more complex. Multipass welding increases this degree of complexity as the previous weld passes and previously affected base metal once again go through a metallurgical change.

2.2.1 Weld Metal Solidification

Due to the high energy input of welding, a thin layer of the base metal is melted but remains unmixed with the weld metal.[7] The newly forming weld metal grains nucleate from the large grains contained in this unmixed zone and grow perpendicular to the fusion line into the center of the weld resulting in a columnar structure.[8] Evidence of this epitaxial growth is not always apparent due to the allotropic transformation that takes place in the fusion zone after solidification.[9] The dendritic growth into the center of the weld is affected by the relationship of the cooling rate to the welding speed as can be seen by observing the direction of the lines on the weld surface and the shape of the weld pool. As this ratio decreases, the weld pool transforms from a circular shape to the shape of a teardrop and becomes increasingly elongated as the travel speed is increased. This is represented schematically in Figure 6.

This shape change is caused by the temperature gradients that exist in the weld metal trailing the arc and the speed in which the arc advances.[9] Grain growth progresses from the fusion line of the weld joint and progresses parallel to the thermal gradient. As the arc moves further along the joint, the temperature gradients curve in behind so that they are always perpendicular to the weld

pool. If one were to only consider an unalloyed metal, growth into the center of the weld would occur only as a function of the removal of heat, whereas effects of adding alloying elements complicate the growth of the solid and the resulting crystalline structure is altered.[8-10] The prevailing growth mode is dependent on the stability of the solid / liquid interface and the solidification structures includes planar growth, cellular growth, or dendritic growth.[8-10] These different growth modes are related to the welding speed by Linnert and are shown schematically in Figure 6.[9]

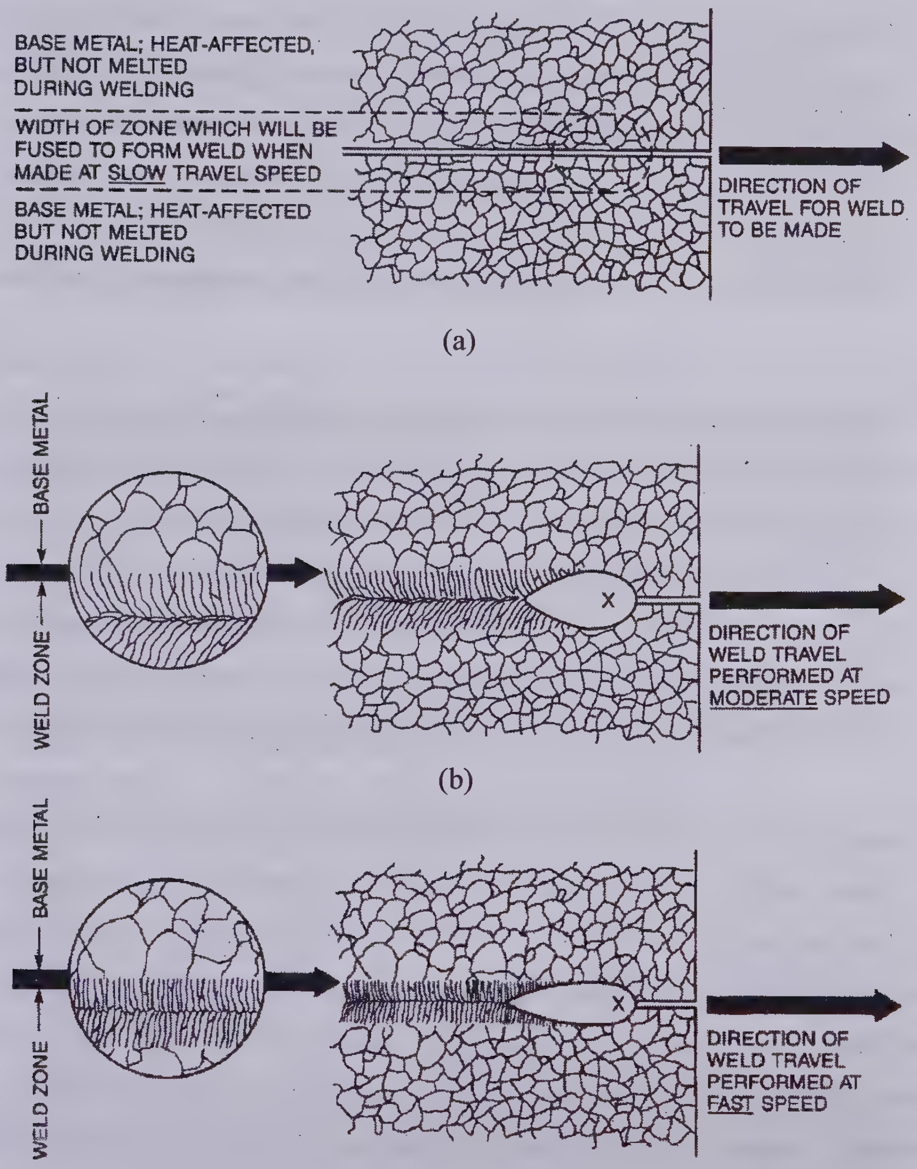
BASE METAL; HEAT-AFFECTED, BUT NOT MELTED DURING WELDING
WIDTH OF ZONE WHICH WILL BE FUSED TO FORM WELD WHEN MADE AT SLOW TRAVEL SPEED
BASE METAL; HEAT-AFFECTED BUT NOT MELTED DURING WELDING
DIRECTION OF TRAVEL FOR WELD TO BE MADE
BASE METAL
WELD ZONE
X
DIRECTION OF WELD TRAVEL PERFORMED AT MODERATE SPEED
BASE METAL
WELD ZONE
X
DIRECTION OF WELD TRAVEL PERFORMED AT FAST SPEED

(a)

(b)

(c)

Fig. 6: Schematic illustration showing effect of welding speed on dendritic growth[9]

When the welding speed is slow the grains are able to form in the planar growth mode as the solid-liquid interface is able to advance into the liquid at a slower pace due to the slow cooling rate. As the speed increases, the cellular mode of growth becomes prevalent as the cooling rate of the weld pool is increased and competitive growth exists at the weld metal / base metal interface. At the higher rate of solidification the resulting cell structure will have higher levels of solute segregation and the advancing solid – liquid interface exists at an increasingly undercooled state where dendritic growth will become more prevalent thereby increasing the amount of elemental segregation. Due to the elongated shape of the weld pool, the dendritic growth will be near perpendicular to the weld centerline. Atomic segregation will tend to the tip of the dendrites as the elements with low melting points are pushed ahead of the solidification front.[5] Alloying elements are typically added to the filler metal to resist solidification cracking (hot cracking) along the weld centerline caused by atomic segregation.

2.2.2 Solid State Transformations in the Weld Metal

After the transformation from liquid to solid, allotropic transformation occurs in carbon and low alloy weld metals where the resulting microstructure is dependant on the cooling rate. Solid state phase transformation in steel is a very well understood metallurgical phenomenon when cooling is slow and the transformation rate considered to be in equilibrium as shown on phase diagrams. In welding, however, the thermal cycle is much more unpredictable as the cooling rate can be rapid and subsequent thermal cycles will occur when welding multiple passes. Basic understanding of the allotropic transformations that occur in iron provide a good background for the reactions in carbon-manganese and low alloy steel welds. In its liquid state, pure iron exists as a face-centered cubic (fcc) structure until solidification at 1530°C where it transforms into a body-centered cubic (bcc) form called delta (δ)-ferrite. At 1394°C, pure iron transforms back into its fcc form, known as austenite or γ-iron, until it reaches 912°C at which point it transforms back into bcc and is known as alpha (α)-iron. The addition of carbon complicates the solidification behavior of iron as can be seen in a Fe-Fe_3C phase diagram where four solid phases exist, α-ferrite, austenite, cementite (Fe_3C), and δ-ferrite. For plain carbon steel the resulting product is primarily a function of the austenitic transformation. In slow cooling conditions the transformation of austenite in plain carbon steel with less than 0.8% C results in what is known as hypoeutectic steel. As the transformation process begins, grain boundary ferrite (proeutectoid ferrite) forms and the excess carbon is rejected into the remaining austenite. As the solubility of carbon decreases with decreasing temperature from 0.02% at 723°C to approximately 0.008% at

room temperature, cementite is formed from the excess carbon.[4] The resulting microstructure is ferrite and pearlite (a mixture of α-ferrite and cementite).

This transformation is not as simple for steel weldments as the cooling rate is much more rapid and the effects of microalloying elements as well as second phase particles must be considered. While the heating phase of the welding process is not generally considered to greatly affect the resulting microstructure, it does have some contribution as higher temperatures cause grain coarsening of the δ-ferrite which promotes large austenite grains on cooling.[11] In addition, the heating rate in a weld is far removed from the equilibrium conditions assumed for phase diagrams, so that dissolution of pearlite and other precipitated phases is incomplete. A high heat input will reduce the cooling rate, thus allowing the weld metal to approach the equilibrium transformation product. This is not considered beneficial, as a product of primarily α-ferrite does not exhibit good strength or impact toughness. Controlling the cooling rate through heat input can allow vast improvements in the mechanical properties. Figure 7 shows the various microstructure formations that may be created by varying the cooling rate.

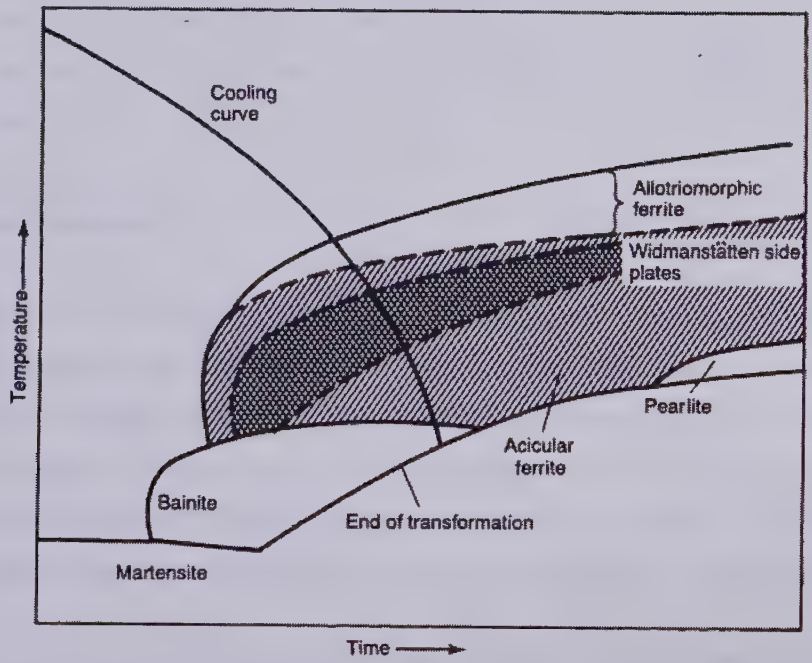

Figure 7: Schematic of weld CCT diagram showing selected microstructures[13]

The cooling rate is generally referred to as $\Delta t_{8\text{-}5}$ (°C/second), which is the time it takes for the weld metal to cool from 800°C to 500°C. This is a direct function of the heat input and the ability of the base metal being welded to remove the heat supplied by the welding arc. If the cooling rate

[illegible]

[illegible]

is too rapid a bainitic or martinsitic microstructure will result, producing a very strong, hard microstructure with poor toughness. As the cooling rate slows, proeutectoid ferrite (allotriomorphic ferrite) is the first to form on the austenite grain boundaries. Ferrite with a Widmanstatten orientation, also known as ferrite side plates, will then nucleate from grain boundary ferrite allotriomorphs along certain crystallographic planes until the grain boundary sites are saturated.[14] When the inclusion content is controlled, acicular ferrite may nucleate at these sites greatly improving the toughness of the weld metal. Studies have found that careful control of the carbon and manganese amounts can produce acicular ferrite levels up to 70% by reducing the volume of proeutectoid ferrite.[14] Acicular ferrite is a fine grained intermediate transformation temperature product that nucleates on inclusions within the austenite grains where ferrite plates radiate in specific directions from the inclusion.[15] This random orientation provides for improved toughness as a propagating crack has a high probability of running into a ferrite plate at a high angle of intersection likely causing the advancing crack to arrest. Carbon-manganese weld metal deposits may also show a variation of another microstructure constituent, ferrite with secondary phases (aligned or non-aligned). Ferrite aligned with secondary phases nucleates at the austenite grain boundaries and grows into the austenite grain where as ferrite with non-aligned secondary phases grows as many small grains with a high aspect ratio.[9] Small amounts of austenite and/or martensite can be retained between the ferrite laths, adversely affecting the toughness.

2.2.3 Alloying Elements

One of the major advantages of flux core welding wire over that of gas metal arc welding is the ability to add alloying elements to the flux in addition to changing the actual metal composition of the welding wire sheath. Specific alloying elements can have a significant influence on arc stability, bead wetting characteristics, weld defects, as well as changing the mechanical properties. Due to the many different influences that alloying elements can have, the various weld metal classifications impose chemical composition requirements to the filler metal.

C	Mn	Si	S	P	Cr*	Ni*	Mo*	V*	Al	Cu
0.18	1.75	0.90	0.03	0.03	0.20	0.50	0.30	0.08	-	0.35

*If not intentionally added, these amounts do not need to be reported.

Table 1: AWS A5.20-95 weld metal chemical composition requirements in maximum weight percent for multipass welds made with an EXT-1(M), E7XT-5(M) and E7XT-9(M)[5]

While carbon additions in weld metal produce a large increase in strength, they also greatly increase the hardness of a metal and reduce toughness. The effect of carbon to produce a hard microstructure, however, can be mitigated by controlling the cooling rate of the weld metal by either increasing the heat input and/or by preheating. Alloying elements, such as manganese, silicon, chromium, molybdenum, and vanadium, can also have an effect on the hardness of the weld metal or heat affected zone by influencing the hardenability of the steel. In order to quantify this effect, a carbon equivalent equation was created to show the effects of carbon and other alloying elements on the hardenability of steel. While many different forms of the equation exists, carbon-manganese and low alloy weld metal follow have shown a good correlation between hardenability and alloy content when using the International Institute of Welding, IIW, equation where,

$$C.E. = \%C + \frac{\%Mn + \%Si}{6} + \frac{\%Cr + \%Mo + \%V}{5} + \frac{\%Cu + \%Ni}{15}$$

As the carbon equivalent increases, the nose of the CCT diagram, such as that shown in Figure 7, will shift to the right and there will be a greater possibility that martensite, a hard brittle microstructure, will form. The alloying elements in the carbon equivalent equation are considered to be austenite stabilizers thus reducing the transformation temperature from austenite to ferrite. If the alloying elements and cooling rate are controlled, however, the transformation temperature may not be reduced enough to allow martensite to form. As stated previously, the desired microstructure is primarily acicular ferrite that with limited amounts of ferrite. If the nose of the CCT diagram is too far to the left, ferrite will be the primary microstructure which will reduce the toughness of the weld metal. The austenite stabilizers in controlled amounts slightly shift the nose to the left and acicular ferrite can form with a controlled cooling rate, either by the natural quenching effect of the base metal or by introducing preheat. These alloying elements also have other beneficial properties in controlled amounts. Manganese is primarily used as a deoxidizer and desulphurizer in the weld pool. Evans has also found that manganese provides a nucleation site for acicular ferrite in amounts up to 1.8% and has an optimal effect on weld metal toughness at 1.5%.[16] It has been seen that the effect of manganese on improving the weld metal toughness is decreased at higher welding currents and cooling times where $\Delta t_{8\text{-}5}$ is greater than 20 seconds.[17,18] Silicon, while also providing a site for acicular ferrite nucleation, has not been found effective enough to offset its ability to increase the strength of weld metal and suppress the

austenite transformation temperature.[19] Nickel has been found to increase the strength of the weld metal and provide a large increase in weld metal toughness. Additions of nickel in amounts as low as 1%, however, will also decrease the operator appeal of the welding electrode as the weld pool is more difficult to control. In significant amounts, nickel has also been found to increase susceptibility to hot cracking due to nickel's tendency to increase the segregation of sulphur during solidification.[7]

2.2.4 Effect of Shielding Gas

Weld metal chemistry can be significantly influenced by the gas-metal reaction occurring during the welding process. These reactions are influenced by the temperature and therefore vary with location within the arc and with the heat input.[21] Flux core arc welding of plain-carbon or low-alloy steel uses gas shielding primarily consisting of 100% CO_2 but can also use an Ar/CO_2 mixed gas varying in amounts of argon from 75% to 95%. Changing the gas composition alters the configuration of the arc plasma. As the amount of argon is increased, the ionization potential is also decreased and the thermal conductivity is decreased. The oxidation potential of the arc decreases with the amount of argon in the plasma.[22] Decreasing the ionization potential allows for a lower voltage at the same current, thus reducing the heat input. Lowering the thermal conductivity creates an arc in which the heat is more intense at the center resulting in a more finger-like penetration profile where the fusion area is narrower at the base.[3] When the product is classified and tested to AWS A5.20 or A5.29, the electrode manufacturer will list the intended shielding gas or give the user a choice of options that will have an influence on operator appeal, arc stability, weld bead appearance, and cost. Many studies have been undertaken to determine the effect of shielding gas composition on flux cored arc welding.[20-25] In addition to changing the welding characteristics, argon has been seen to have a profound effect on the resulting mechanical properties of the weld metal.

CO_2 is an active shielding gas component that will react in the arc and break down to the following:

$$CO_2 \rightarrow CO + O_2$$

The amount of oxygen available from the breakdown of CO_2 increases with an increase in heat input thereby raising the oxidizing potential of the arc.[23] While some of this oxygen will remain

as a solid solution, much of this available oxygen will then form with manganese and silicon from the consumable according to the following,[21-25]

$$Si + 2O \rightarrow SiO_2$$
$$2Mn + 2O \rightarrow 2MnO$$

As the weld metal cools, silicon and manganese oxides precipitate out of the weld metal and into the slag. The remaining oxygen forms oxides thereby increasing the amount of inclusions which provide nucleation sites at the grain boundaries for the formation of proeutectoid ferrite.[24] As a result, the weld metal will exhibit decreased toughness[22-24].

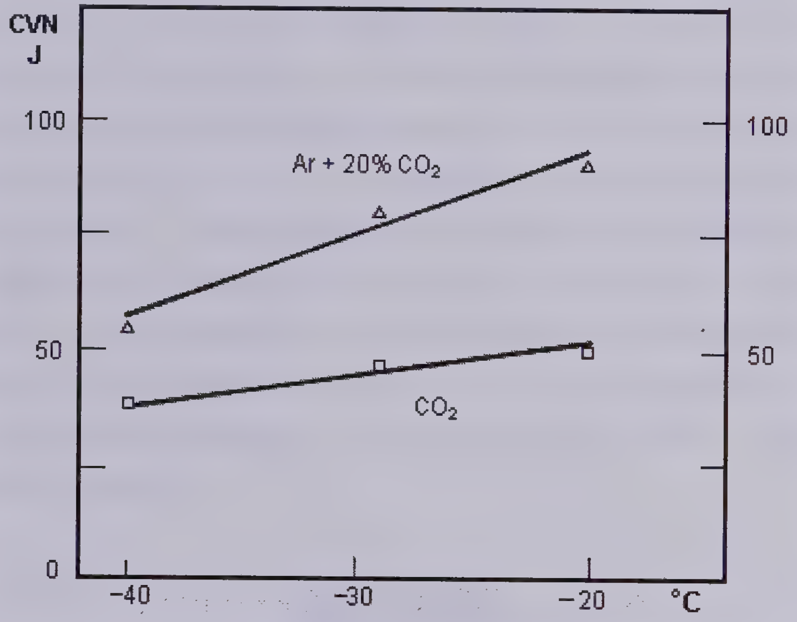

Fig. 8: Shielding gas effect on Charpy V-notch impact toughness[25]

Addition of argon to the shielding gas has a positive influence on arc stability, decreases the amount of oxygen found in the weld metal, lowers the volume of grain boundary ferrite, and promotes the formation of acicular ferrite, thus improving toughness.[22,24] Due to the lower oxygen content the amount of manganese and silicon content in the weld metal increases with an increasing amount of argon in the shielding gas.[22,24] This addition of argon also reduces the penetration and changes the penetration profile to be finger-like. At higher amounts of argon, the resulting weld will become increasingly narrow at the base and the penetration will be reduced.

Many flux-cored consumables contain additions to the flux in order to facilitate arc stability when used with 100% CO_2. Due to the microstructural changes between different consumables of the same classification with changing argon percentages, this study focused on welding with 100% CO_2. This is also the primary shielding gas used with flux-cored electrodes due to the cost savings when compared with the higher priced Ar/CO_2 blends.

2.2.5 The Heat Affected Zone

The heat affected zone, or "HAZ", is the region of the base metal adjacent to the weld metal deposited in which a change in the microstructure or mechanical properties has occurred as a result of welding. This area is of great concern as the base metal has undergone a series of rolling operations and carefully controlled heat treatments to obtain the mechanical properties required by the specification to which it conforms. While peak temperatures reaching only as high as 100°C can have an affect on the mechanical properties of the base metal, significant changes occur within the coarse grain HAZ and the fine grain HAZ where the peak temperatures reached are generally much higher.[7] The coarse grain HAZ is the most visibly changed area as the peak temperature reached is just lower than the melting point of the metal at the fusion line and reduces as you move away from the fusion line. High peak temperatures promote austenite grain growth, which will result in larger ferrite grains on cooling. The coarse grain HAZ is known to be the part of the HAZ that often exhibits the greatest increase in tensile strength and greatest decrease in fracture toughness.

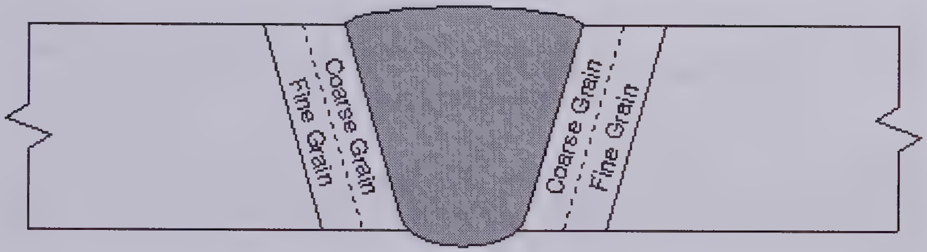

Fig. 9: Weld metal with heat affected zone

Due to the short time it takes for the energy to be transferred to the base metal, structural segregations that exist within the microstructure may retain their composition after cooling.[7] The primary concern in this area is the amount of grain coarsening and the speed in which the heat is dissipated. If the $\Delta t_{8\text{-}5}$ is low, a martinsitic or bainitic microstructure may result as seen in Figure 7. The change that occurs in this region is very dependant on the alloying elements present in the

steel and the condition of the microstructure prior to welding. The HAZ is generally regarded as the critical area that should be investigated for a decrease in impact properties due to the unknown result of welding on the material microstructure. With the increasing demand for steel from the international market, most steels used in the structural steel industry are produced for conformance to many different grades and the impact properties of the material is often much greater than that required for structural applications. Figure 10 shows the impact test results of 100 plates provided to conform to CSA G40.20/40.21, 350WT Cat. 4 (impact testing requires 27J at -45°C) ranging in thickness from 20mm to 38mm. As can be seen, the probability that the impact toughness far exceeds that required is great. For this reason, the material being used should be evaluated prior to determining the weld procedure as the toughness reduction in the HAZ may not be a primary concern due to the high initial toughness of the base material.

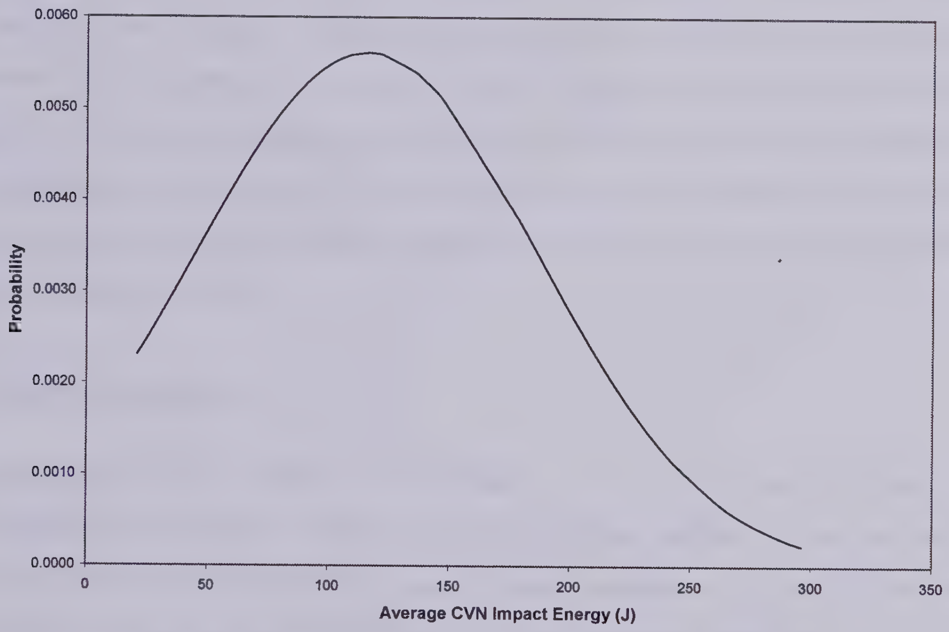

Fig. 10: Normal distribution for Charpy V-notch impact energies of CSA G40.21 350WT Cat. 4 plate

2.3 Fracture

Materials used in steel construction are chosen by the designer to handle the specified loads and resist fracture. Structural design codes provide a framework for avoiding failure by analyzing the forces present and select the material shapes and sizes to resist these forces.[27] Occasionally, however, fracture is inevitable despite designing within the code requirements and a material must be chosen in which the behavior of that metal can be predicted for the specific application.

In all cases, brittle failure must be avoided. Much of the information needed can be found from a simple tensile test of the material, where the yield strength, tensile strength, and ductility can be determined, forming the basis of most standard design criteria. While design standards often give load resisting properties for various material section sizes, taking into account the statistical probability of variations in the material dimensions and mechanical properties, they do not account for possible stress concentrations that may result in a crack propagating through a component.

Unfortunately, most design codes consider that material response to loading or, in some cases, overloading will be ductile in nature and will not act in a brittle manner. Advances in material processing have enabled the designer to rely on structural grade steels to be supplied with a limited number of inclusions or defects that may prove harmful to a structure. The primary concern, rather, is the fabrication of the steel sections into useable structural members. It is in this processing phase that the steel undergoes rework, creating flaws that may not be tolerated in the design due to the increased stress levels associated with the flaw. While manufacturing codes and standards impose quality control measures that reduce the chances of detrimental flaws existing in a structural member, critical components need to be more carefully examined and fracture mechanics considered.

2.3.1 Fracture Toughness

The fracture toughness of a material is its resistance to the advancement of a crack. When a defect in the form of a notch or a crack exists within or on the surface of a material, the resulting stresses in the vicinity of this defect far exceed those experienced throughout the rest of the material. Fracture toughness may be defined in different manners depending on the stress-strain response of the material. If the material acts in an elastic manner, linear elastic fracture mechanics, LEFM, principles govern. In most cases the steel used in structural applications exhibit plastic deformation at the crack tip and elastic-plastic fracture mechanics, EPFM, may be used to evaluate a materials response to crack initiation and propagation.[28]

In LEFM a stress intensity factor, K, is used in quantifying the magnitude of the local crack tip stresses as illustrated in Figure 11.

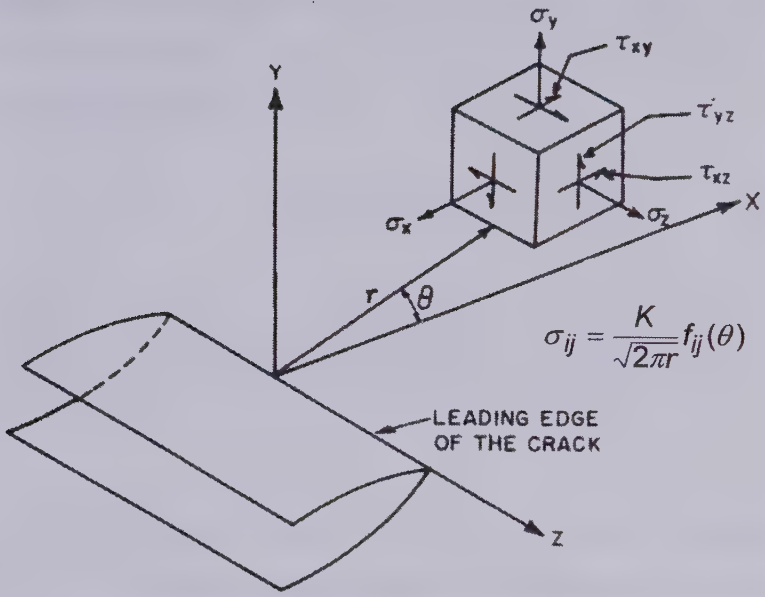
σ_y
τ_{xy}
τ_{yz}
τ_{xz}
X
Y
σ_x
σ_z
r
θ
$\sigma_{ij} = \frac{K}{\sqrt{2\pi r}} f_{ij}(\theta)$
LEADING EDGE OF THE CRACK
Z

Fig. 11: Stress components ahead of a crack[29]

If the component is thin the material will be allowed to move in the Z direction and $\sigma_Z \approx 0$ thus creating a plane stress condition. If the component is sufficiently thick, a plane strain condition will exist where the movement in the Z direction is constrained creating a triaxial state of stress at the crack tip. Plane strain is more severe than plane stress and is the governing condition.

There are three different loading modes that affect the propagation of a crack.

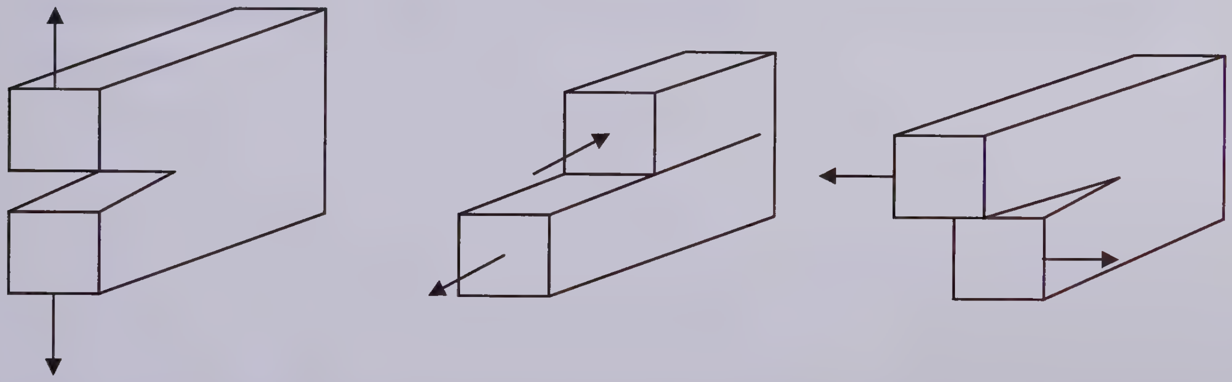

Mode I: Opening (tension) Mode II: In-plane shear Mode III: Out-of-plane shear

Fig. 12: Crack Tip Loading Modes

The most commonly seen single loading case is mode I where the crack is opened as the load is applied normal to the crack plane. The stress intensity factor for mode I loading can be determined for the loading and geometry by:

$$K_I = \beta\sigma\sqrt{\pi a}$$

Once a material in plane strain mode I loading experiences a combination of stress and flaw size that creates unstable fracture, the critical stress intensity, K_{IC}, has been reached. The critical K value will be higher in the case of plane stress and is denoted as K_C.

In EPFM, a plastic zone immediately ahead of the crack is considered and the resulting resistance to crack propagation is increased. As the crack tip experiences both elastic and plastic deformation, the fracture parameter must now take these two stress-strain responses into consideration. Both the J contour integral and the crack-tip-opening displacement, CTOD, are used to quantify crack tip conditions in EPFM.

Generally, a materials stress-strain curve will follow the Ramberg-Osgood relationship where

$$\varepsilon = \frac{\sigma}{\mathrm{E}} + \frac{\sigma^n}{F} \quad \left(\varepsilon = \varepsilon_{el} + \varepsilon_{pl}\right)$$

Using this relationship, the J contour integral can be broken down into an elastic and a plastic portion where:

$$J = J_{el} + J_{pl}$$

$$J_{el} = \frac{K^2}{E},$$

$$J_{pl} = \frac{H\sigma^{n+1}a}{F}$$

In 1961 an alternative method was presented for quantifying the elastic-plastic response at the crack tip of a material as it was noticed that the opening at the crack tip (caused by blunting) increased with the increased fracture toughness of the material.[29] It was proposed that the fracture behavior could be related to the amount of crack tip blunting a material has experienced at the exact moment of fracture, known as the crack-tip opening displacement. This idea has been

further developed to show a relationship between the crack opening at the mouth, COD, and the CTOD.

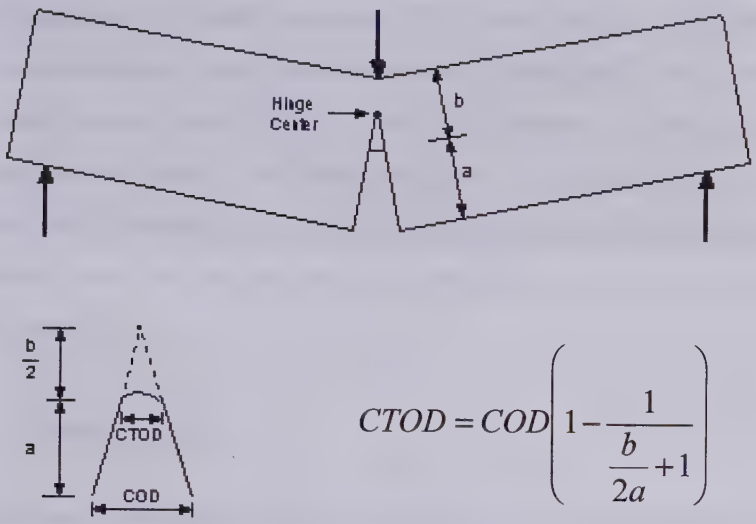

$$CTOD = COD\left(1-\frac{1}{\frac{b}{2a}+1}\right)$$

Figure 13: Crack opening displacement test and inferred CTOD[29]

Since this discovery, a mathematical relationship has been developed relating the CTOD to both the K and J parameters.

$$CTOD \approx \frac{K^2}{E\sigma_{ys}} \quad \text{(LEFM)}$$

$$CTOD \approx \frac{J}{\sigma_{ys}} \quad \text{(EPFM)}$$

Many standardized test methods have been developed to quantify the fracture toughness of a material by various internationally recognized organizations. The American Society for Testing and Materials (ASTM), the British Standards Institute (BSI), and the International Institute of Standards are a few of the world-renowned organizations that publish such standards. Within the ASTM standards there are many different test configurations that are permitted for use with relation to a specific standard.

ASTM standard E1820-01, Standard Test Method for Measurement of Fracture Toughness, provides methods to evaluate K, J, and CTOD for metals from a load-displacement record. This standard gives the user the option of using different test specimen configurations, all of which

have been pre-cracked through cyclic loading to ensure that the specimen contains a reasonable representation of a naturally occurring crack. Once the specimen is loaded, stable crack propagation should commence giving what is known as an R-curve showing the relationship between fracture toughness and crack extension. If the crack reaches the point where unstable crack extension occurs, the point value at this instance is considered to be the fracture toughness of the material. While testing directly for K, J, or CTOD parameters is the most accurate way to characterize a material's response to an advancing crack, this testing is very costly due to the large specimen size and the number of variables that need to be satisfied to produce accurate data. If the original testing shows that the dimensional criterion is not met, the test must be repeated until the criterion is met.

2.3.2 Charpy V-Notch Impact Test

The Charpy V-notch test, developed in the early 1900's, was used to correlate static and dynamic test results for materials.[32] During World War II a large number of U.S. Navy ships, the Liberty ships, were developing large cracks in their hull. Many of these fractured locations were found to start at an area where a notch existed due to design and fabrication methods, but it was found that the crack would, in some cases, arrest in members that showed an increase in Charpy V-notch impact energies and a decrease in the transition temperature of the metal.[29,32] The U.S. National Bureau of Standards Report, 1948, established that the transition temperature of the metals corresponded with a minimum 27 Joules (15 ft.lbs) Charpy V-notch impact test result.[33] This value is still used extensively as the minimum impact requirement for structural steels in most applications. Gross has since found that the energy absorbed in a Charpy V-notch test corresponding to the transition temperature increases with increasing yield strength of the metal.[18] For this reason, many of the standards relating to material requirements call for increasing impact energies with increasing yield strengths as can be found in the Canadian Standards Association G40.21 and AWS D1.5.[26,48] The Charpy V-notch impact test, while used frequently because of the speed and low expense in which testing can be carried out, has some limitations when used to evaluate the fracture response of metals. The specimen size, standardized under ASTM E23-02A, Standard Test Methods for Notched Bar Impact Testing of Metallic Materials, has the dimensions of 10mm x 10mm x 55mm long. This places the material in a condition of plane stress whereby the specimen is not thick enough to preclude lateral shrinkage thereby inducing only a biaxial state of stress at the crack tip. For this reason, a crack in the same material that is much larger in size will experience a triaxial state of stress at a crack tip and will propagate at lower stresses.

Secondly, the Charpy V-notch test involves machining a groove into the specimen resulting in a blunt notch rather than a crack. The test results are dependant on the individual laboratories equipment for creating this notch and the resulting radius at the crack tip may vary from one laboratory to another. Finally, the test method used involves striking the sample with a swinging pendulum causing fast fracture. The results will vary significantly with those seen when the load is applied slowly under quasistatic conditions as in the test to determine K, J, or the CTOD.[29,32,35] Because of these inconsistencies in test methods, numerous studies have been undertaken to develop a relationship between the information obtained in a fracture toughness test and that obtained in a Charpy V-notch test.

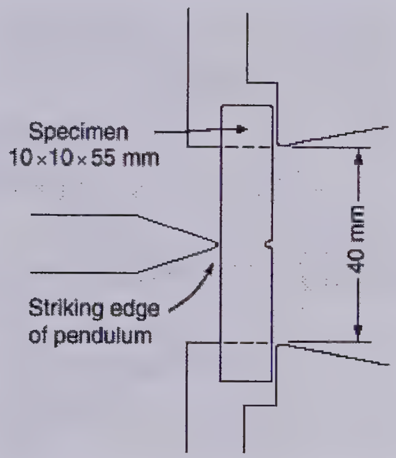

Fig. 14: Charpy V-notch general testing configuration[36]

The Charpy V-notch data may be divided into three distinct regions, the lower shelf, the transition region, and the upper shelf. The mathematical relationships developed between Charpy V-notch data and fracture toughness parameters depend on the region within the data that the corresponding fracture toughness is desired.

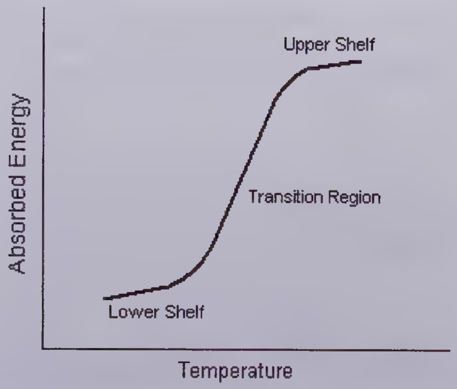

Fig. 15: Typical Charpy V-notch test behavior for structural steels

It has been shown that the transition region in the Charpy V-notch data occurs in the same temperature range as that found from testing the impact plane-strain fracture toughness, K_{ID}.[37] Testing to determine K_{ID} requires an increase in the loading rate used when testing for K_{IC}. ASTM E1820-01 requires a loading rate that results in the maximum load being obtained in 0.1 – 10 minutes for determination of K_{IC}. When testing for the impact fracture toughness, this loading rate is increased significantly shifting the test data to the right.[29]

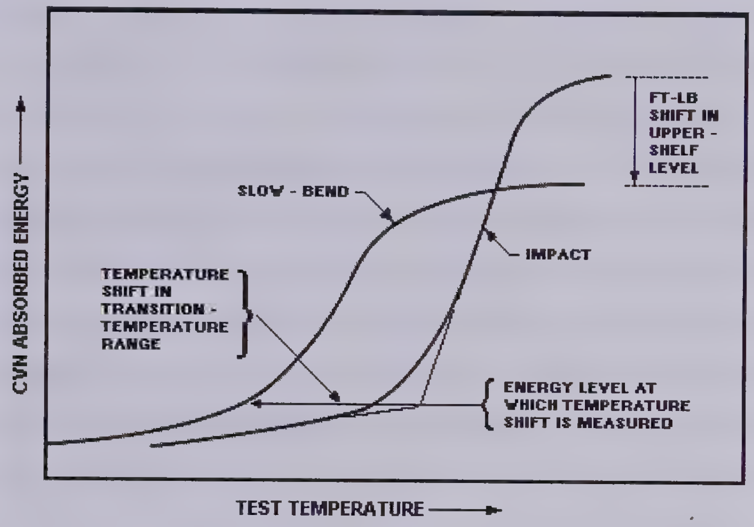

Fig. 16: Effect of strain rate on Charpy V-notch impact data[38]

Barsom and Rolfe have found that a dynamic impact plane strain, K_{ID}, must first be calculated from the CVN data and then a shift in temperature calculated at which this result also represents the K_{IC} values.[29] This method has been shown to allow conversion from CVN data to K_{IC} data in the transition region for steels with a yield strength between 36 – 140 ksi (248 – 965 MPa).

$$\frac{(K_{ID})^2}{E} = 5 \cdot CVN\,(ft \cdot lbs)$$

$$T_{shift}(^\circ F) = 215 - 1.5\sigma_{ys}(ksi)$$

British Standard BS 7910:1999 uses the following correlation for predicting the material toughness measured by the stress intensity factor from CVN data in the lower shelf and transition region.[38]

$$K_{mat}\left(N/mm^2\right) = \frac{820\sqrt{CVN(J)} - 1{,}420}{B^{1/4}(mm)} + 630$$

2.3.3 Application of Charpy V-Notch Test Results

Many steel fabrication codes give acceptance / rejection criteria for flaws in either the base material or the welds according to whether the loading condition is static or dynamic, tensile or compressive.[26,35,37] These values are given in terms of physical size for inspection using radiography, or by the reflection of acoustic frequencies when using ultrasonic testing. These acceptance criteria, however, are general in nature and are usually conservative. Use of steels with improved fracture toughness and special loading conditions, whether more or less severe, can change the applicability of the allowed flaw size. To determine the required fracture toughness for a structure or whether an existing flaw will be deleterious to a structure, an engineering assessment may be performed. British Standard BS 7910:1999, Guide on Methods for Assessing the Acceptability of Flaws in Metallic Structures, requires that the engineer calculate loading conditions for the structure and subject these to factors in the design that create stress concentrations as well as fabrication and erection tolerances that also contribute to increasing local stresses. For weld zones, residual stresses must also be considered, as these lead to an increase in the local stresses around a welded joint. BS 7910:1999 allows for differing levels of detail by providing three levels of assessment that correspond with the reliability of the data entered. If the material properties are based on the material specifications or from testing other similar samples, giving typical results, possible errors in this input must be taken into consideration and the resulting acceptance level will be more stringent to account for the uncertainty. In addition to this, the degree to which an existing flaw can be evaluated with regards to orientation and size also has an effect on the reliability of the input data. Once an assessment level has been determined as outlined in the Standard, the engineer may calculate the stress intensity factor, K. This may then be used to determine the required impact toughness of the material, as determined through Charpy V-notch testing, by using the rudimentary relationship as given in the previous section.

3.0 MATERIALS AND EXPERIMENTAL PROCEDURE

The present investigation is designed to study the effects of varying the heat input on the microstructure and Charpy V-notch impact properties of the weld metal. Maintaining a consistent travel speed and changing the current and voltage is used to vary the heat input. The test samples were allowed to cool below 100°C prior to welding the subsequent pass. After welding at three different heat inputs, the samples underwent a Charpy V-notch test, were examined macroscopically and microscopically, and were tested for hardness in the different zones. A larger wire size, from the same manufacturer, was then tested to determine if there was a significant difference in the impact testing results and to allow the heat input to increase further than that possible with the first wire size. The two welding wires underwent an all-weld-metal chemical analysis to ensure that the effect of varying alloying elements could be accounted for in deciphering the data. Charpy V-notch impact tests were performed on all samples at three different temperatures located near the transition temperature of the weld metal.

3.1 Welding Equipment

The welding power source used was a Lincoln DC-600, 3 phase CC/CV welding machine capable of 600 amps at 100% duty cycle. The wire feeder used was a 4-drive roll type to ensure consistent feed rates. The welding gun was placed on an automated travel carriage to allow steady arc travel and a consistent travel time. Power output readings were taken by a Amprobe ACDC 3000 ammeter . The current was found to vary from that shown on the power source by up to +5%, which was deemed acceptable. The voltage was taken at the arc to eliminate any losses due to connections and the power cables.

3.2 Welding Consumables

FCAW welding wire classified as AWS A5.20, E70T-1, -9 in both 1.6mm diameter and 2.4mm diameter, is used. The results of a chemical analysis completed on both wires according to ASTM E1019-02, E1097-97, and E1479-99 is contained in Appendix A. The shielding gas for the chemical analysis test and the present test was 100% CO_2.

3.3 Base Metal

The base metal consists of 2 - 25mm plates, each cut 300mm long x 150mm wide. A single-vee weld joint with a 30° included angle, no land, and a 10mm root opening on a 10mm steel backing bar was used. The plate was tested in accordance with CSA G40.20/40.21 Grade 350WT Cat. 4. The chemical composition is contained in Appendix A.

3.4 Welding Data

The parameters of each test run were recorded and are contained in Appendix B.

3.5 Charpy V-Notch testing

The Charpy V-notch test was conducted using a pendulum type machine. Sample preparation and testing was in accordance with ASTM E23-02a using a full size, 10mm x 10mm x 55mm sample, with a machined notch 2mm deep at a 45° included angle and a tip radius of 0.25mm. Impact data was obtained with the notch at the centerline of the weld metal as shown in Appendix C.

All welding conditions were impact tested using 3 samples at 3 different temperatures, -34°C (-30°F), -40°C (-40°F), and -46°C (-50°F).

3.6 Metallography

Appendix D contains both the macrostructures and microstructures from each of the plates welded with the 1.6mm welding wire. The macrostructures are obtained by surface grinding with a 600 μm surface grinder and etching with a 10% Nital mixture. The microstructural evaluation is performed after surface polishing with a diamond paste polisher and etching with a 2% Nital mixture. A picral etch is performed using 10% picric acid in order to observe any secondary phases present.

4.0 RESULTS AND DISCUSSION

It was observed that the lowest heat input for the 1.6mm wire gives the worst impact test results for all temperatures. The highest heat input when welding on the 25mm plate, however, gives the best results at the two lower temperatures and only a slightly lower result than the intermediate heat input at the -34°C test temperature. When the interpass temperature was not controlled, the impact values at a heat input of 2.0 kJ/mm decreased slightly from those obtained when the interpass temperature was controlled, but still outperformed the toughness of the weld made at a heat input of 1.5 kJ/mm.

When comparing these results with those obtained from the larger 2.4mm wire it is seen that at the same heat input, the impact test results vary. At a heat input of 1.5 kJ/mm the 2.4mm wire is seen to have the best impact properties for the -34°C and -46°C temperatures, but drops significantly at the -40°C test temperature. A heat input of 2.6 kJ/mm does not drop as rapidly as the other two test cases but seems to maintain a linear drop from the highest to lowest temperature. The heat input of 2.0 kJ/mm gave the worst result for the 2.4mm wire while this heat input gave the best result for the 1.6mm wire. In addition to the results mentioned above, there is no reliable trend indicating whether the 1.6mm diameter wire will produce better Charpy V-notch impact test values than the 2.4mm wire. The 2.4mm wire provides significantly improved impact toughness at the -34°C and -46°C temperatures but is equal at the -40°C temperature when welding at a heat input of 1.5 kJ/mm. At a heat input of 2.0 kJ/mm the opposite is seen and the 1.6mm wire shows improved toughness values at all temperatures.

The trends within each test group generally show a decrease of impact energy with the decrease of testing temperature. Some scatter, however, does exist, which is consistent with the results obtained from Charpy V-notch testing of weld metal and may also be attributed to the notch location within the different microstructures. As can be seen from the macrostructures and microstructures a small difference in notch location can result in testing an area in which a completely different microstructure is prevalent. The theory enabling prediction of primary microstructures of welds is well established and shows definite trends relating microstructure to toughness.[38,39] During multipass welding a portion of the previous weld pass is reheated and may undergo microstructural transformations which rely on the peak temperature reached and cooling rate. The region that is affected by subsequent weld passes may only be tempered, annealed or, if the temperature is sufficient, this region of weld metal may be re-austenitized.[39-42] It has been

found that this reheated area can have significantly varying toughness results depending on the microstructural changes that occur for which many theories have attempted to predict.[38-41,43,44] Changes in the primary weld microstructure may include grain coarsening, a decrease in defect density, and precipitation of carbides.[41] Due to the inability of easily predicting the reaction of the primary weld metal microstructure to the subsequent heat input, the resulting mechanical properties are determined from empirical testing.

The macrostructures for the 1.6mm wire are presented in Appendix D showing the pass / layer sequence and the various zones that are created within a weld. The heat affected zone is evident in all welds as are the areas showing primary weld metal and reheat zones created from subsequent weld passes. The reheat zone in the weld completed with a heat input of 2.0 kJ/mm is the most prominent as the peak temperature would have been the greatest in this weld. The reheat zone in the lowest heat input weld, 1.0 kJ/mm, is the least prominent as the peak temperature would have been the smallest in this weld. When evaluating the hardness test results, found in Appendix E, it is seen that the hardness of the reheated area is less than that of the primary weld microstructure. The resulting impact results are therefore dependant on both the microstructure in the primary weld metal as well as the reheat zone. These microstructures are a direct result of peak temperature reached in the primary metal, cooling rate of the primary weld metal, peak temperature reached due to subsequent weld passes, and the cooling rate of the reheat zone. The following explanation can be hypothesized from this reasoning. At a low heat input of 1.0 kJ/mm the resulting weld is composed mostly of primary weld metal as the peak temperature is not very high and the relative amount of reheat zone is minimal. The cooling rate resulting from this heat input is not sufficient enough to produce a martensitic microstructure, as can be seen from the low hardness values obtained from the weld metal. The toughness results show that the resulting weld has adequate toughness. When the heat input is increased to 1.5 kJ/mm, the resulting reheat zone is still not large enough to sufficiently offset the reduction in toughness due to the resulting grain coarsening of the primary weld metal microstructure. This results in a weld metal with reduced toughness from that seen when welding at a heat input of 1.0 kJ/mm. When the heat input is further increased to 2.0 kJ/mm, the resulting reheat zone of the weld increased considerably in volume fraction of the weld joint as can be seen in the macrostructure of the weld. This increase in reheated area resulted in an increase in toughness as seen with the Charpy V-notch test. When the interpass temperature is not controlled, the amount of annealed weld metal is increased, resulting in a decrease in toughness from that seen when the interpass temperature is controlled at a maximum value of 100°C prior to putting any subsequent weld passes. This

annealing effect also creates a more homogeneous microstructure throughout the weld zone resulting in a decrease in the scatter commonly found from Charpy V-notch testing.[40]

Appendix D contains the microstructures of the welds made with the 1.6mm electrode. The microstructure of the weld metal deposited with a heat input of 1.0 kJ/mm shows a relatively fine-grained structure of polygonal ferrite with acicular ferrite. The picral etch shows unaligned secondary phases. At the higher heat input of 1.5 kJ/mm the there are more concentrated regions of ferrite with coarse acicular ferrite. More secondary phases are also present than at the lower heat input as seen with the picral etch. The highest heat input of 2.0 kJ/mm produced a microstructure with acicular ferrite and less polygonal ferrite which is more finely dispersed. Grain coarsening can be seen in the welded joint as the heat input increased and where the interpass temperature was not controlled.

5.0 CONCLUSIONS

As can be seen from the results of the impact testing, presented in Appendix C, no clear trend is available to help predict weld metal toughness behavior at different heat inputs. The Charpy V-notch data gathered from the testing of the different wire sizes at the varying temperatures does not provide results showing a decrease in Charpy V-notch results with an increase of heat input. This relationship has typically been observed in other similar studies.[44-46] When viewing the microstructures, however, it is seen that the impact toughness results correlate with the microstructures present in the weld metal. In addition to this, the different impact test results between the 1.6mm wire and the 2.4mm wire can be, in part, attributed to the notch location with respect to the pass/layer sequence. As was explained earlier, the current density with a smaller wire size will allow more metal to be deposited at the same heat input as a larger wire size. This will change the location of the untempered and reheat zones in the weld metal. For this reason, the test may be optimized by creating a pass/layer sequence that will give the optimum toughness at the region in which the notch is made for toughness testing. It must be noted that the resulting Charpy V-notch values will not be indicative of the entire weld zone.

The use of Charpy V-notch results at one set of parameters or heat input does not guarantee that the results will follow any clear trend to another heat input whether greater or smaller. It is a requirement of AWS D1.1, Structural Welding Code – Steel, that procedures qualified to produce certain Charpy V-notch impact values are still valid if the heat input is reduced but not increased. It is a requirement of AWS D1.5, Bridge Welding Code, that the heat input must not be increased by more than 10% or decreased by more than 30%. As was shown in this study, a reduction in heat input cannot be relied upon to maintain a minimum toughness level when the weld is made in multiple passes/layers. The degree of reaustenitization must be taken into consideration as this will change when the heat input is decreased and the degree of grain coarsening must be controlled.

The well known relationship between heat input and the amount of grain coarsening in the heat affected zone can be seen from the microstructures in Appendix F. It has been well documented that at a higher heat input, the HAZ will exhibit reduced toughness. For this reason, the material being welded must be evaluated prior to welding in order to determine whether there is a reason for concern if the heat input is increased. With the increase on demand of the steel mills material is being produced in mass quantities to enable use in a wide range of applications where the

toughness requirements may be much greater than that required by the structural steel industry. Figure 10 shows the wide range of toughness values achieved from material certified in accordance with producing Charpy V-notch values of 27 Joules at -45°C. Where the toughness of the material being used is many times greater than that required, it is most likely that this will not be the limiting factor when developing a weld procedure at a reasonable heat input. The specific material must be examined prior to determining the weld procedures to be used and the area that will most likely cause the greatest concern. Despite this, toughness testing of the HAZ should be carried out to ensure that steps taken to improve the toughness of the weld metal has not decreased the toughness in the HAZ to a dangerously low level.

6.0 FUTURE WORK

The work done in this study shows that conventional knowledge regarding primary weld zones cannot be relied upon in producing the best resulting weld when multiple passes/layers are used. Further work needs to be done to help predict the resulting microstructures and their volume fraction in multipass welding. Determining peak temperatures and cooling rates from subsequent welding passes at set heat input values, preheat and interpass temperatures, as well as material thicknesses, will help further the knowledge in this area. Due to the effect that alloying elements have on the resulting microstructure, however, the results from such tests would most likely be constrained to a very limited number of cases.

7.0 REFERENCES

1. Milner, D.R., Salter, G.R., and Wilkinson, J.B. Arc Characteristics and their Significance in Welding. British Welding Journal 7 (2) 1963, pp 73-88.

2. The Procedure Handbook of Arc Welding, The Lincoln Electric Company, 1994.

3. Welding Handbook, 8th ed., Volume 2, AWS, 1991.

4. Smith, W.F. Structure and Properties of Engineering Alloys, 2nd edition. McGraw-Hill, U.S.A. 1993.

5. American Welding Society Specification A5.20, Carbon Steel Electrodes for Flux Cored Arc Welding

6. American Welding Society Specification A5.29, Low-Alloy Steel Electrodes for Flux Cored Arc Welding

7. Patchett, B.M. Casti Metals Blue Book, 3rd edition. Casti Publishing. 2000.

8. David, S.A. and Vitek, J.M. Principles of Weld Solidification and Microstructures. International Trends in Welding Science and Technology: Proceedings of the 3rd International Conference on Trends in Welding Research, Gatlinburg, TN, June 1-5, 1992, pp 147-156.

9. Linnert, G.E. Welding Metallurgy: Carbon and Alloy Steels, Vol 1, 4th edition. American Welding Society, 1994, pp 786-891.

10. Trivedi, R. and Kurz, W. Heat Flow Conditions. ASM Handbook, Volume 15, Solidification of Single-Phase Alloys. ASM International,1993.

11. Gooch, T.G. and Hart, P.H.M. Solid State Phase Transformations in Steel During Welding. Advances in Welding Science and Technology: Proceedings of an International Conference on Trends in Welding Research, Gatlinburg, TN, May 18-22, 1986. Ed. S.A. David, pp 161-176.

12. P. Ravi Vishnu, Solid State Transformations in Weldments, ASM Handbook Vol. 6 Welding, Brazing, and Soldering. ASM International. 1993.

13. Bhadesia, H.K.D.H. Diffusional Formation of Ferrite in Iron and its Alloys. Progress in Materials Science Vol. 29. pp 321-386. 1985.

14. Svensson, L.-E. and Gretoft, B. Microstructure and Impact Toughness of C-Mn Weld Metals. Welding Journal Vol 69 (12), 1990, pp 454s – 461s.

15. Bhadeshia, H.K.D.H. Models for Acicular Ferrite. International Trends in Welding Research, eds. S. A. David and J. M. Vitek, ASM International, Ohio, USA, 1992, pp. 213-222.

16. Evans, G.M. Effect of Manganese on the Microstructure and Properties of All-Weld-Metal Deposits, Welding Journal Vol 59(3), 1980. pp 67s-75s.

17. Dixon, B. Evaluation of Consumables and Development of Procedures for Optimum Toughness in Submarine Steels. An International Conference on Materials in Welding and Joining. Institute of Metals and Materials Australasia Ltd, 1995, pp 31-36.

18. Kasatkin, O.G. and Seiffert, B. Dependance of the Fracture Toughness of Low- and Medium-Alloyed Weld Metal on its Composition and Structure. Paton Welding Journal Vol 6 (3), 1994, pp 175-178

19. Evans, G.M., The Effects of Sulphur and Phosphorus on the Microstructure and Properties of C-Mn All-Weld-Metal Deposits, IIW Doc. II-A-630-84

20. Onsoien, Morten I. Shielding Gas Oxygen Equivalent in Weld Metal Microstructure Optimization, M.Sc. Thesis, Colorado School of Mines, March 1994.

21. Meyendorf, N. Metal Gas Reactions in Gas-Shielded Welding. Welding International, No. 7, 1998, pp 653-657.

22. Ramanathan et al. Effect of Shielding Gas on Fusion Characteristics and Weld Metal Properties in Flux Cored Arc Welding. Trends in Welding Research, Proc. of the 4th Int'l Conf., June 1995.

23. Lathabai, S. and Stout, R.D., Effect of Shielding Gas Composition and Heat Input on the Notch Toughness of Flux-Cored Weld Metal. WRC Progress Report, Vol. 39 (2), pp 7-18, 1984.

24. Ramini de Ressone et al. Effect of Welding Procedure (welding position, number of layers, arc energy, and shielding gas type) on ANSI/AWS A5.20-95 E71T1 Flux Cored Wire Deposits. Science and Technology of Welding and Joining, Vol. 8 (2) 2003.

25. Stenbacka, N. and Persson, K.A. Shielding Gases for Gas Metal Arc Welding. Welding Journal, November 1989, pp 41-47.

26. National Standard of Canada CAN/CSA - G40.20-04/G40.21-04, General Requirements for Rolled or Welded Structural Quality Steel / Structural Quality Steels. Canadian Standards Association, 2004

27. Kulak, J and Grondin, G., Limit States Design in Structural Steel, 7th ed., CISC, Willowdale, ON. 2002.

28. Anderson, T.L. Fracture Mechanics Fundamentals and Applications 2nd Ed. CRC Press, 1995.

29. Barsom, J.M, Rolfe, S.T. Fracture and Fatigue Control in Structures: Applications of Fracture Mechanics, ASTM, West Conshohocken, PA. 1999.

30. Wells, A.A., "Unstable Crack Propagation in Metals – Cleavage and Fast Fracture: Cranfield Crack Propagation Symposium, Vol. 1, September 1961, p.210.

31. ASTM Standard E1820-01, Standard Test Method for Measurement of Fracture Toughness.

32. Toth, L, Rossmanith, H.P., and Siewert, T.A. Historical Background and Development of the Charpy Test. From Charpy to Present Impact Testing. Eds D. Francois and A. Pineau. Elsevier Science Ltd and ESIS. 2002, pp 3-19.

33. Williams, M.L. and Ellinger, G.A. Investigation of Fractured Steel Plates Removed from Welded Ships. National Bureau of Standards Report, December 9, 1948.

34. Gross, J.H. Effect of Strength and Thickness on Notch Ductility. Impact Testing of Metals, ASTM STP 466, 1970, pp 21-49.

35. Hertzberg, R.W. Deformation and Fracture Mechanics of Engineering Materials. John Wiley & Sons, Inc. U.S.A. 1996.

36. ASM Handbook Vol 8 Mechanical Testing and Evaluation. ASM International. 2000

37. Barsom, J.M. and Rolfe, S.T., "The Correlations Between K_{IC} and Charpy V-notch Test Results in the Transition-Temperature Range," Impact Testing of Metals, ASTM STP 466, 1970, pp 281-302.

38. Strangwood, M. and Bhadeshia, H.K.D.H. Segregation, Oxygen Content and the Transformation Start Temperature in Steel Weld Deposits. Proceedings of an International Conference on Welding Metallurgy of Structural Steels. Published by The Metallurgical Society of the AIME, Warrendale, Pennsylvania. Ed. Koo, J.Y., 1987, pp 495-504

39. Yang, J.R. and Bhadeshia, H.K.D.H. Reaustenitisation in Steel Weld Deposits. Proceedings of an International Conference on Welding Metallurgy of Structural Steels. Published by The Metallurgical Society of the AIME, Warrendale, Pennsylvania. Ed. Koo, J.Y., 1987, pp 549-563

40. Reed, R.C. and Bhadesia, H.K.D.H. Complete Reaustenitisation in Multirun Steel Weld Deposits. Recent Trends in Welding Science and Technology. ASM International, Ohio. Ed. David, S.A. and Vitek, J.M., 1989, pp 205-210.

41. Mythili, R. et al. Microstructural Modification Due to Reheating in Multipass Manual Metal Arc Welds of 9Cr-1Mo Steel. Journal of Nuclear Materials Vol 312, 2003, pp 199-206.

42. Yang, J.R. and Bhadeshia, H.K.D.H. Reaustenitization Experiments on Some High-Strength Steel Weld Deposits. Materials Science and Engineering Vol A118, 1989, pp 155-170.

43. Rorvik, G, Onsoien, MI, Kluken, AO, and Akselsen, OM. High Heat Input Welding of Offshore Structures – Procedures and Weld Properties. Welding Journal Vol 71(9), 1992. pp331s – 339s

44. Kasatkin, O. and Seiffert, B. Depenance of the Fracture Toughness of Low and Medium-Alloyed Weld Metal on its Composition and Structure, Paton Welding Journal, Vol 6(3), 1994. pp 175-178.

45. Prasad Rao, K and Janvir, B.K. Effect of Microstructure on Mechanical Properties of C-Mn Weld Metal, Praktische Metallographie 25, 1988. pp 214-224

46. Yongyuth, P. et al. Influence of Macro/Microstructure on the Toughness of "All Weld" Multipass Submerged Arc Welded C-Mn Steel Deposits, ISIJ International, Vol. 32(6), 1992. pp 771-778

47. American Welding Society AWS D1.1-2004

48. American Welding Society AWS D1.5

49. British Standard BS7910:1999

50. Anderson, Ted L., "Fracture Mechanics," Engineering Handbook, edited by Dorf, Richard, CRC Press, Boca Raton, FL, 1998, Ch 11.

51. Krauss, G. Iron-Carbon Phase Diagram. ASM Handbook Vol. 1 Properties and Selection: Irons, Steels, and High Performance Alloys. 1990

52. Broek, D. The Practical Use of Fracture Mechanics. Kluwer Academic Publishers, Netherlands, 1989.

53. Lyttle, K.A. Shielding Gases for Welding. ASM Handbook Vol 6, Welding, Brazing, and Soldering. ASM International. 1993.

54. Rice, J.R. A Path Independent Integral and the Approximate Analysis of Strain Concentration by Notches and Cracks. Journal of Applied Mechanics, Transactions ASME, Vol 35, June 1968.

55. Grong, O. and Matlock, D.K. Microstructural Development in Mild and Low Alloy Steel Weld Metals, International Metals Reviews Vol 31(1), 1986. pp 27-48

8.0 APPENDICES

APPENDIX A

Material Chemical Compositions

Weld Metal Chemical Analysis

1.6mm E70T-1, -9, S/N 63059, 100% CO_2 shielding gas

Total Carbon	0.028 %
Manganese	1.75 %
Phosphorus	< 0.01 %
Sulphur	0.006 %
Silicon	0.71 %

2.4mm E70T-1, -9, S/N 62831, 100% CO_2 shielding gas

Total Carbon	0.029 %
Manganese	1.39 %
Phosphorous	< 0.01 %
Sulphur	0.007 %
Silicon	0.49 %

Base material test data

25mm plate, CSA-G40.21-98 Grade 350WT CAT 4.
Supplied by Stelco Hamilton

Heat number 870164

Chemical analysis

Carbon	0.15	%
Manganese	1.35	%
Phosphorous	0.11	%
Sulphur	0.003	%
Silicon	0.30	%
Copper	0.015	%
Nickel	0.19	%
Chromium	0.022	%
Molybdenum	0.004	%
Vanadium	0.06	%
Columbium	0.020	%
Titanium	0.008	%
Tin	0.002	%
Soluble Aluminum	0.035	%

Mechanical Testing

Yield Strength	453 MPa
Tensile Strength	574 MPa
% Elongation	25

Charpy V-notch data at -45°C:	Sample 1	149 Joules	Ave = 149 Joules
	Sample 2	139 Joules	
	Sample 3	158 Joules	

APPENDIX B

Welding Data

Plate Number	Plate Thickness (mm)	Wire Size (mm)	Max Interpass Temperature	Amperage	Voltage	Travel Speed (mm/sec)	Gas Flow (m^3/hr.)
1	25	2.4	100°C	350	28.5	6.8	1
2	25	2.4	100°C	450	30.6	6.8	1
3	25	2.4	100°C	550	32	6.8	1
5	25	1.6	100°C	250	27.2	6.8	1
6	25	1.6	100°C	330	30.5	6.8	1
7	25	1.6	100°C	430	32	6.8	1
10	25	1.6	None	430	32	6.8	1

Table B1: Welding Data

APPENDIX C

Charpy V-Notch Data

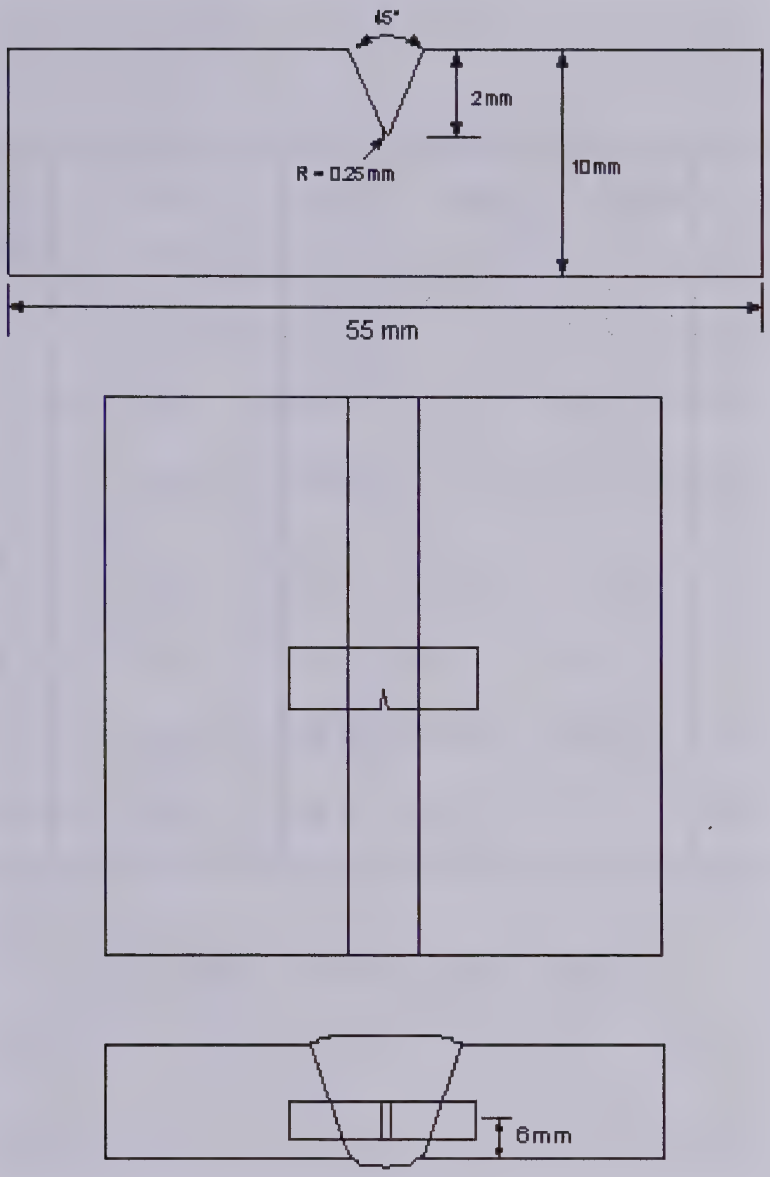

Fig. C1: Charpy V-notch specimen location

Plate Number	Heat Input (kJ/mm)	-34ºC			AVE	-40ºC			AVE	-46ºC			AVE
1	1.47	48.8	46.1	52.1	**49.0**	21.2	23.1	18.2	**20.8**	30.9	42.3	22.5	**31.9**
2	2.03	42.6	30.9	30.6	**34.7**	16.5	17.9	23.9	**19.4**	24.4	17.9	25.5	**22.6**
3	2.60	43.7	33.9	35.3	**37.6**	24.7	35.3	43.4	**34.5**	23.1	31.5	14.9	**23.2**
5	1.00	43.1	38.0	47.7	**42.9**	21.2	29.6	34.2	**28.3**	24.7	26.4	20.6	**23.9**
6	1.49	24.4	19.3	20.3	**21.3**	25.5	21.7	20.3	**22.5**	17.6	22.0	19.3	**19.6**
7	2.03	45.0	42.6	40.1	**42.6**	62.4	36.9	55.3	**51.5**	28.2	23.1	32.3	**27.9**
10	2.03	55.1	29.8	25.5	**36.8**	33.9	48.8	21.7	**34.8**	15.2	44.7	20.9	**26.9**

Table C1: CVN Impact Data (Joules)

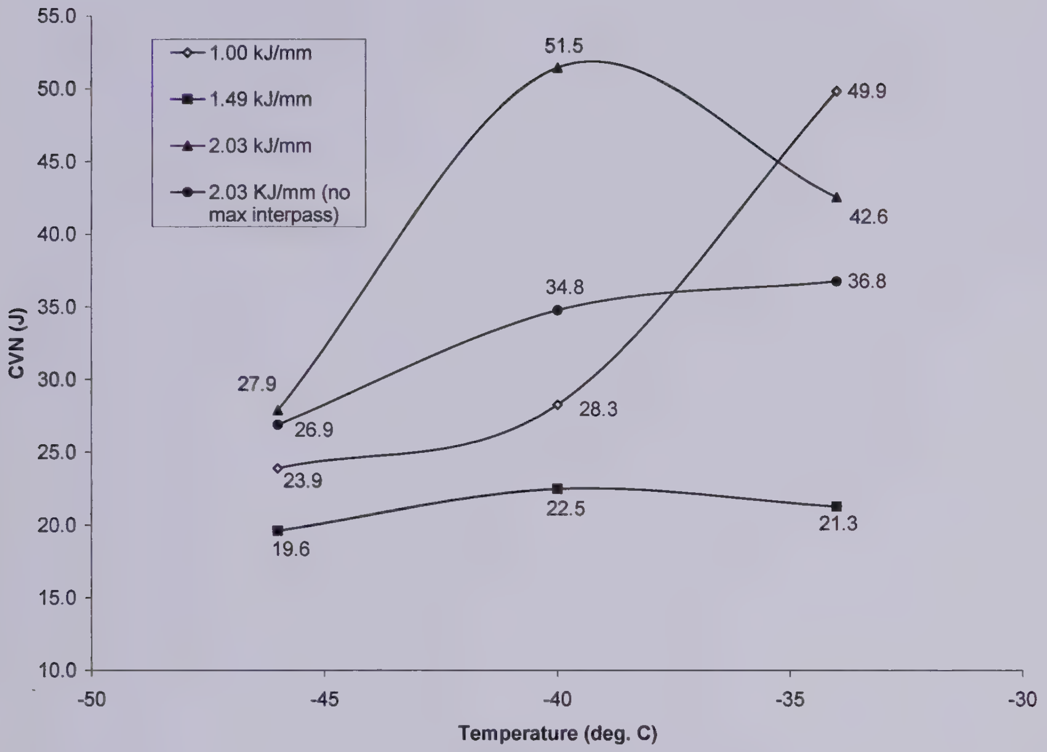

Fig C2: CVN Impact Values (Joules) for 1.6mm Welding Wire

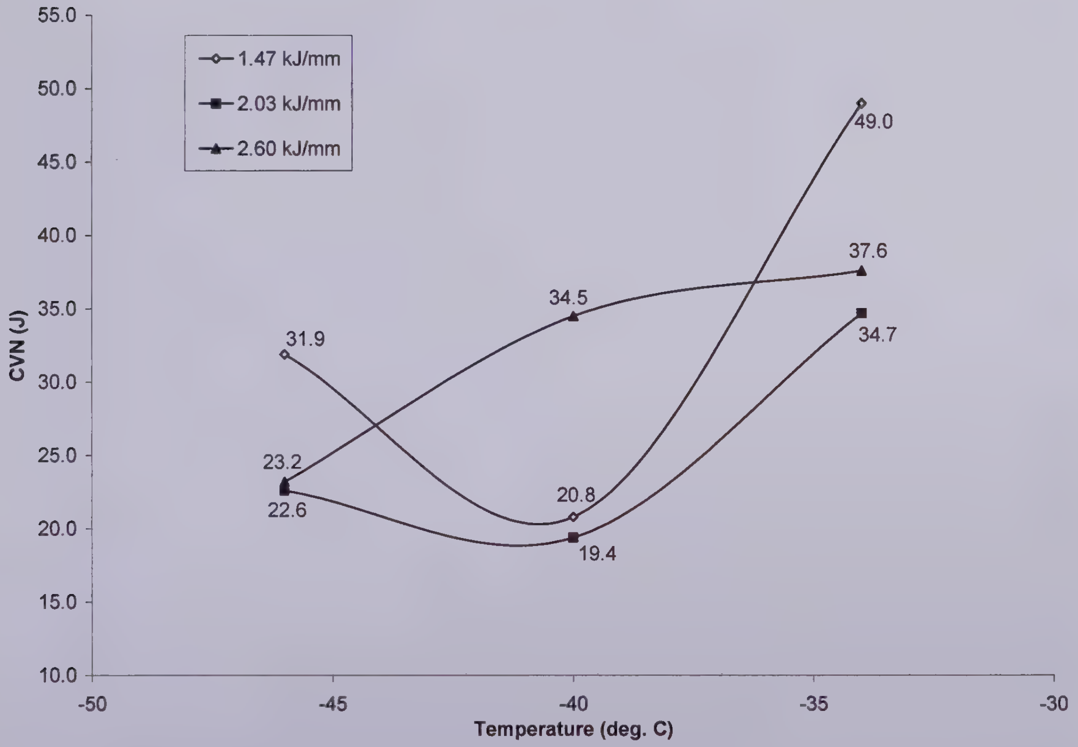

Fig C3: CVN Impact Values (Joules) for 2.4mm Welding Wire

APPENDIX D

Metallography

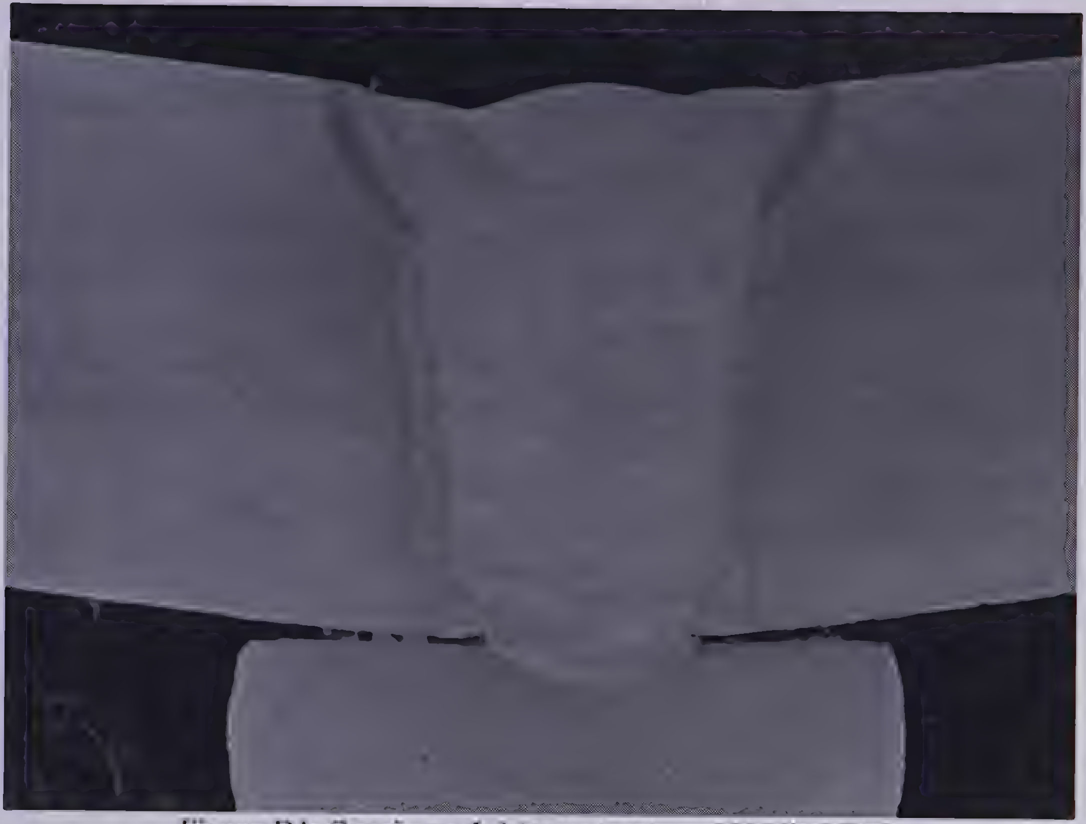

Figure D1: Specimen 5, Macrostructure, 2% Nital Etch

Figure D2: Specimen 5, Weld Metal Microstructure, 2% Nital Etch, 400x Magnification

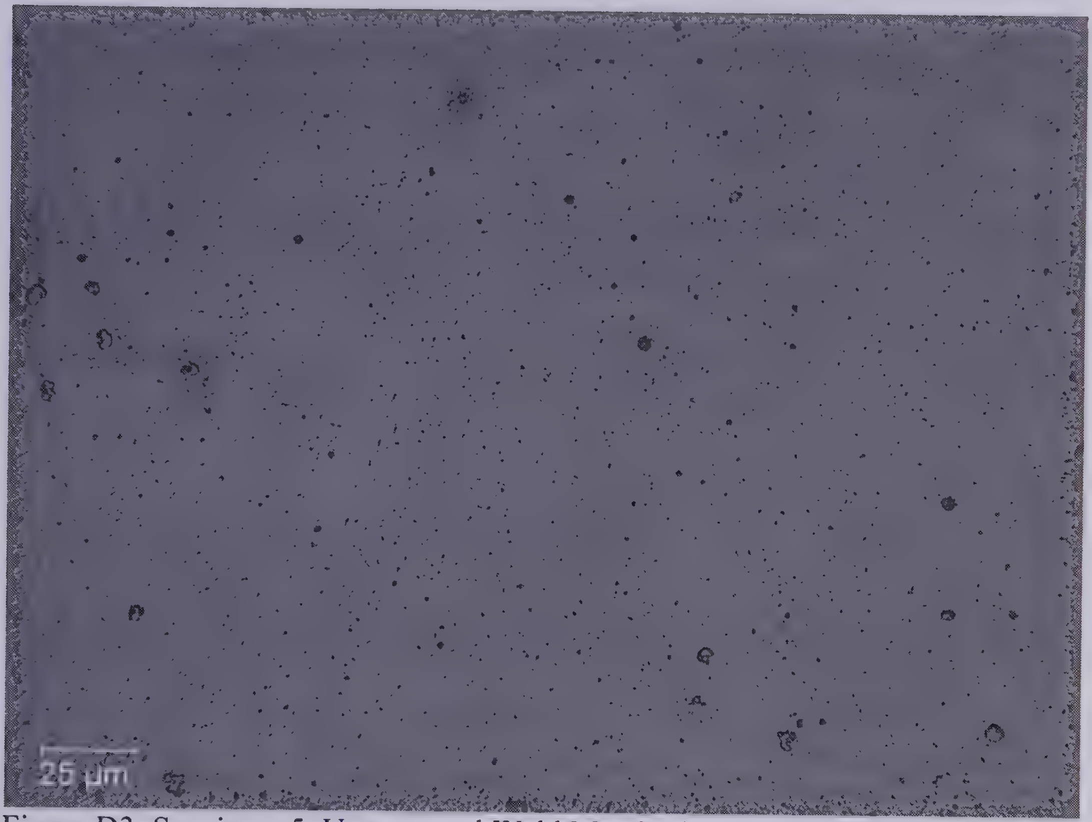

Figure D3: Specimen 5, Untempered Weld Metal, Picral Etch, 400x Magnification

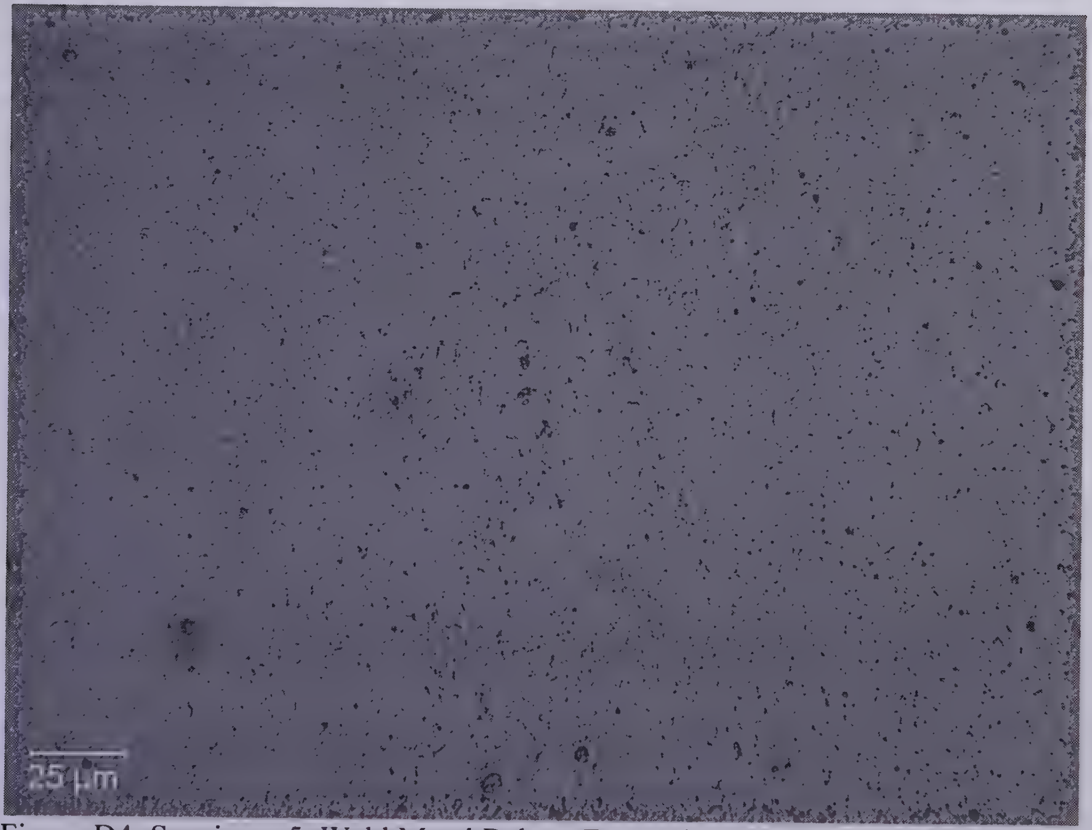

Figure D4: Specimen 5, Weld Metal Reheat Zone, Picral Etch, 400x Magnification

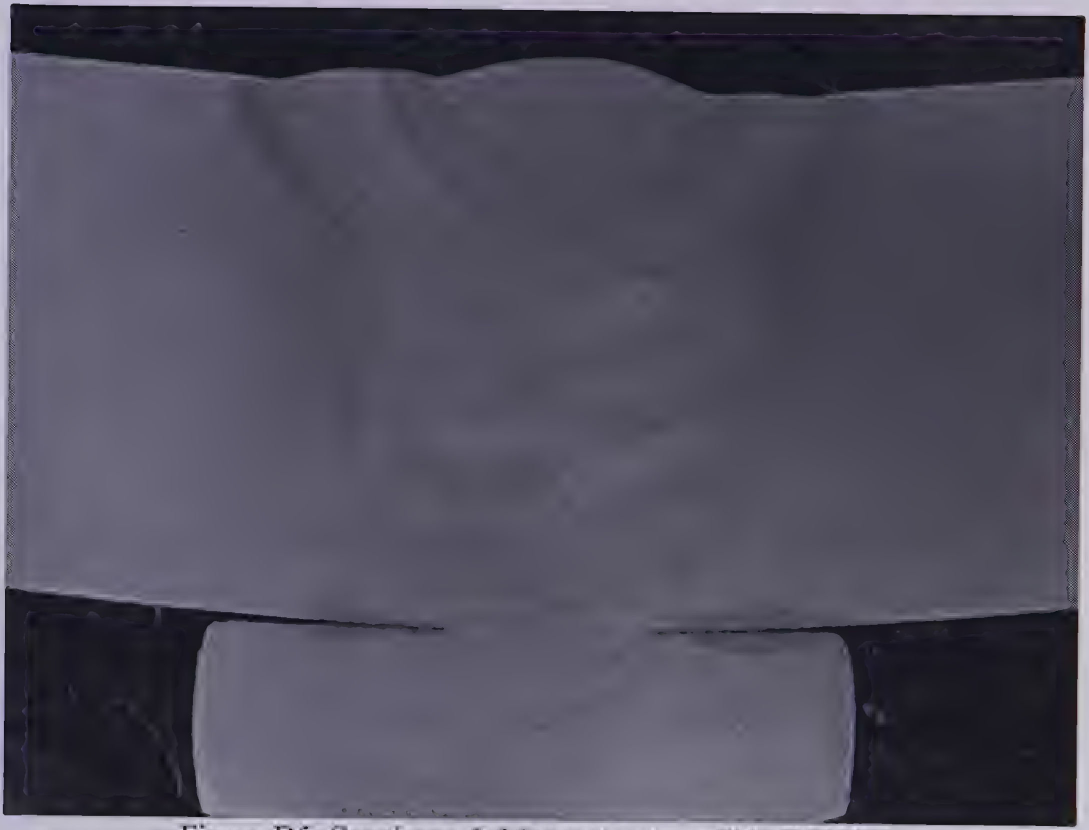

Figure D5: Specimen 6, Macrostructure, 2% Nital Etch

Figure D6: Specimen 6, Weld Metal Microstructure, 2% Nital Etch, 400x Magnification

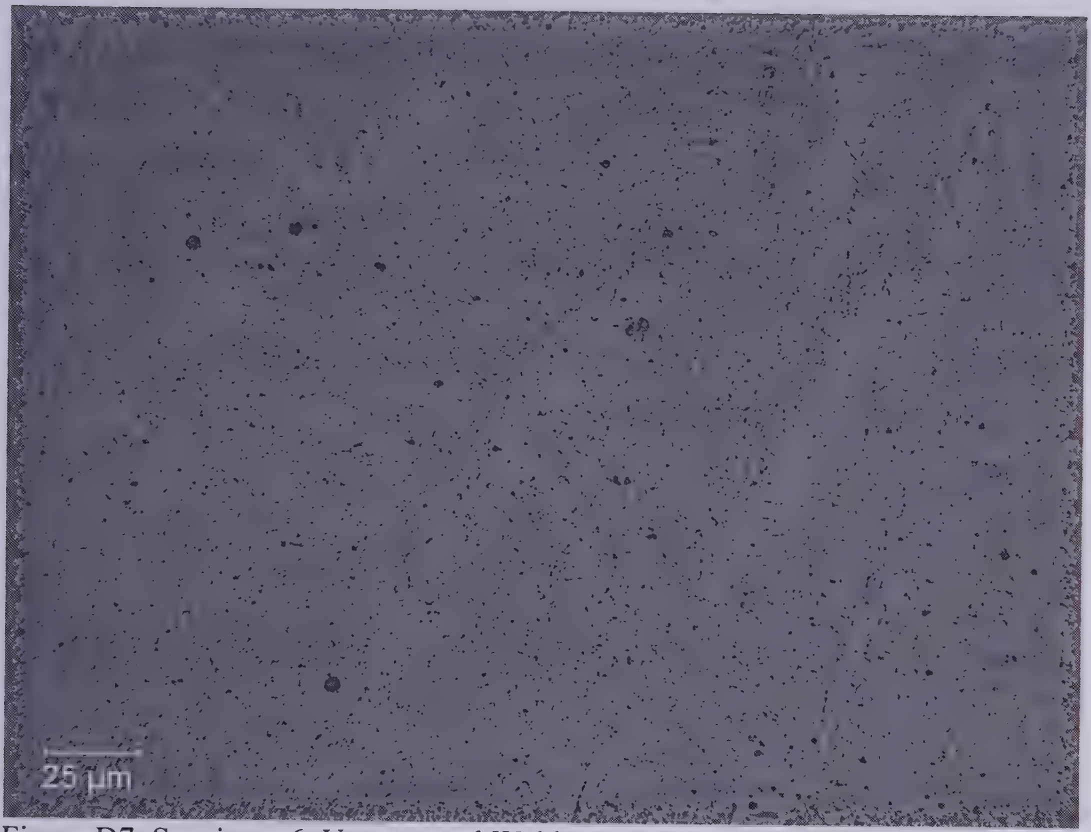

Figure D7: Specimen 6, Untempered Weld Metal, Picral Etch, 400x Magnification

Figure D8: Specimen 6, Weld Metal Reheat Zone, Picral Etch, 400x Magnification

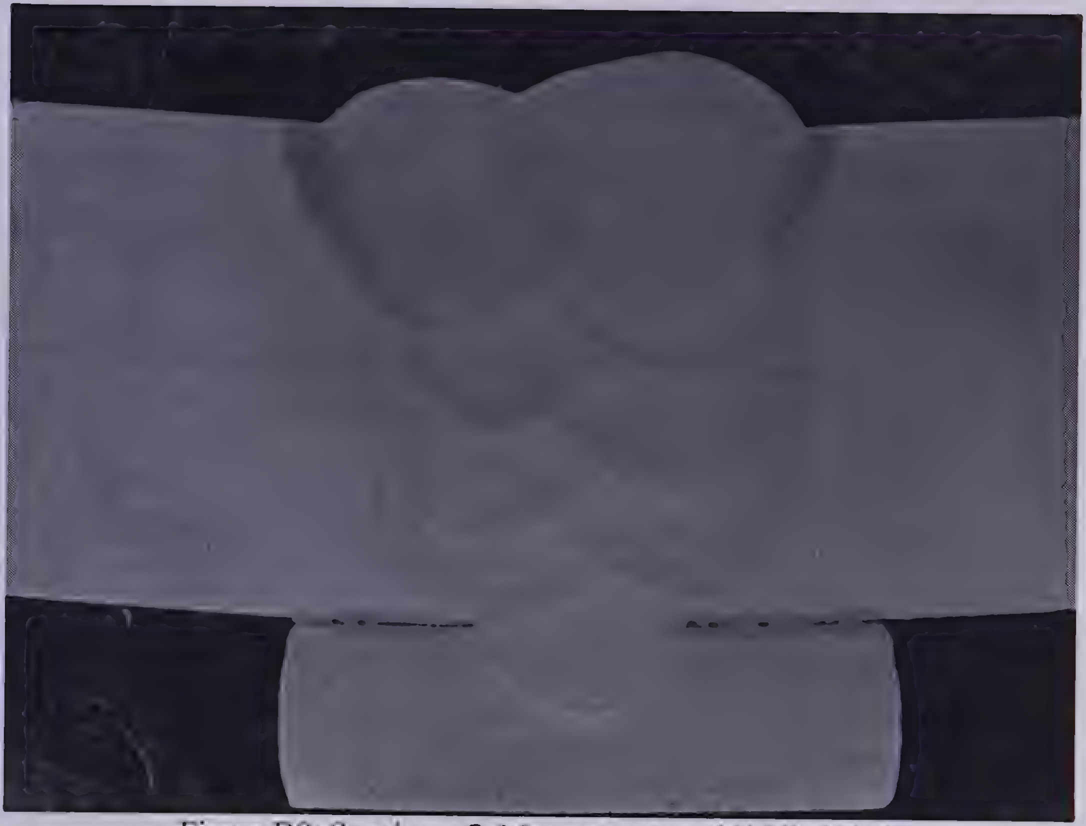

Figure D9: Specimen 7, Macrostructure, 2% Nital Etch

Figure D10: Specimen 7, Weld Metal Microstructure, 2% Nital Etch, 400x Magnification

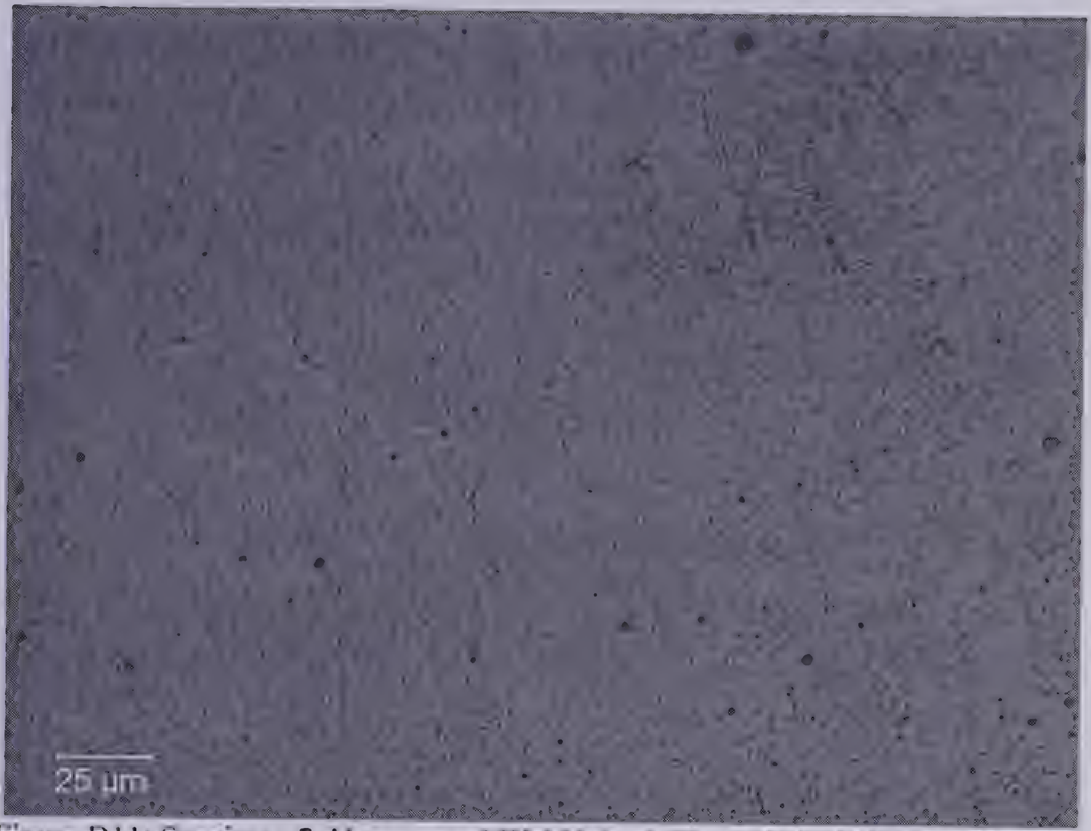

Figure D11: Specimen 7, Untempered Weld Metal, Picral Etch, 400x Magnification

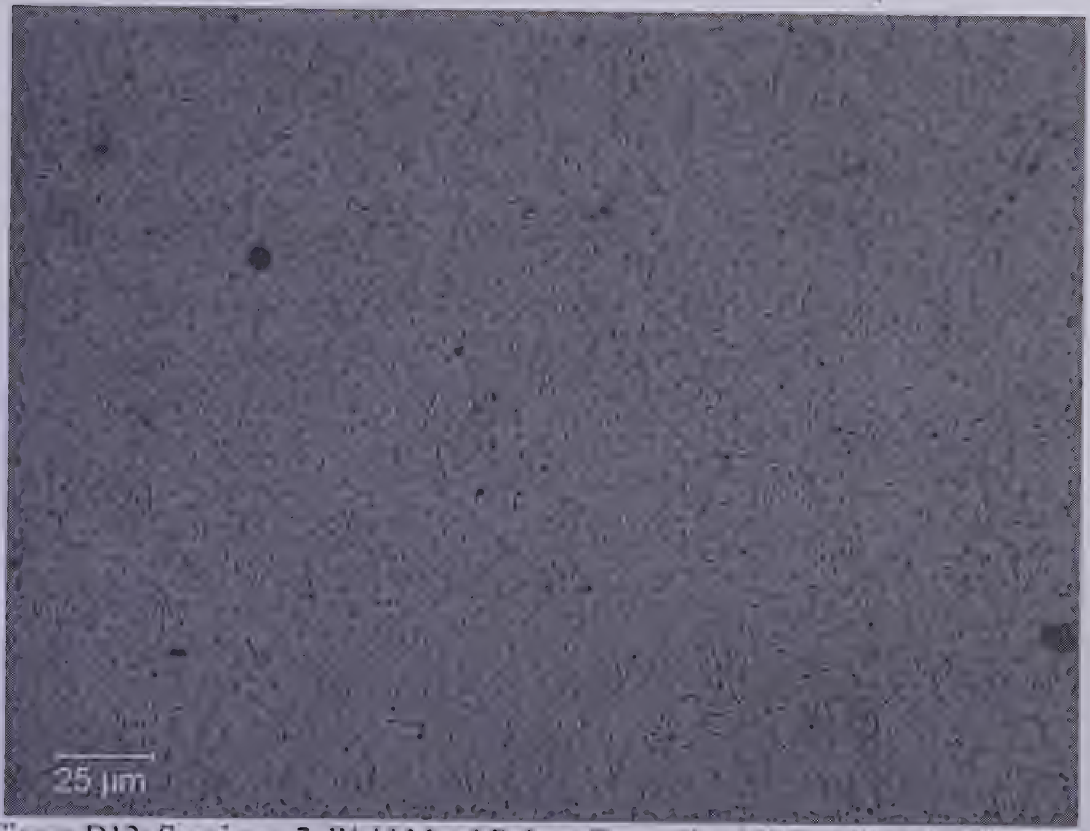

Figure D12: Specimen 7, Weld Metal Reheat Zone, Picral Etch, 400x Magnification

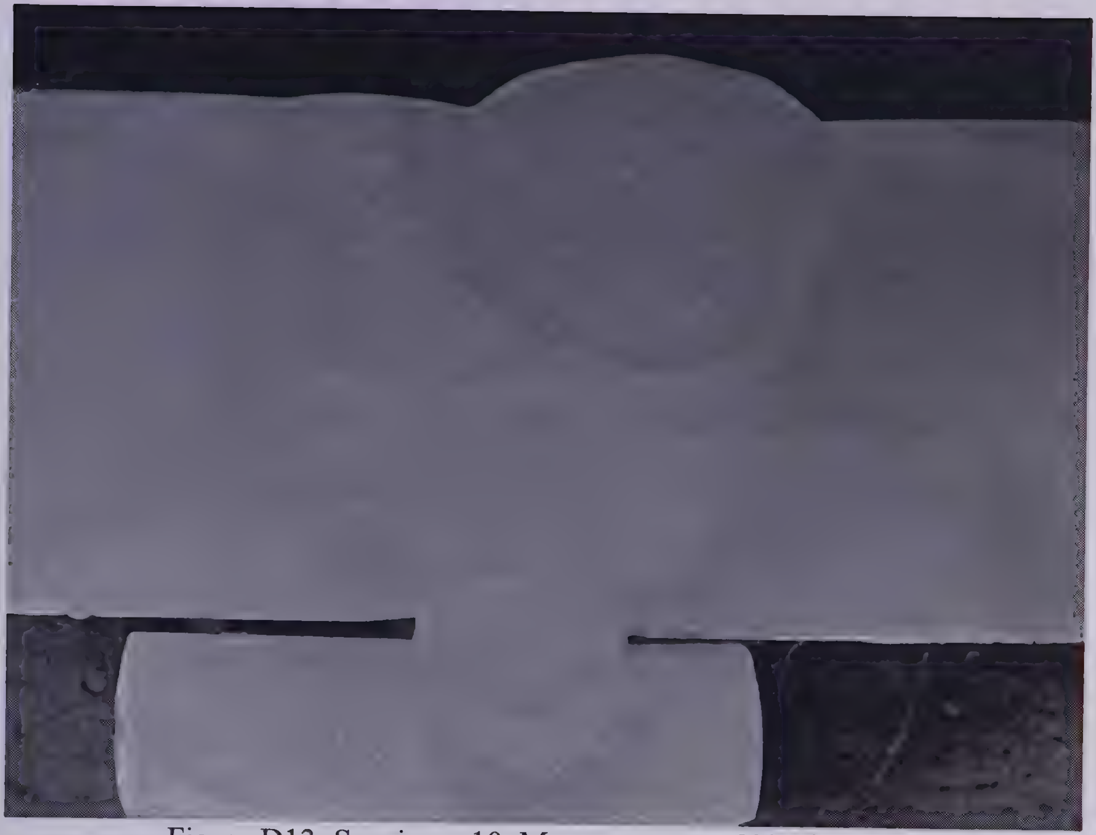

Figure D13: Specimen 10, Macrostructure, 2% Nital Etch

Figure D14: Specimen 7, Weld Metal Microstructure, 2% Nital Etch, 400x Magnification

Figure D15: Specimen 10, Untempered Weld Metal, Picral Etch, 400x Magnification

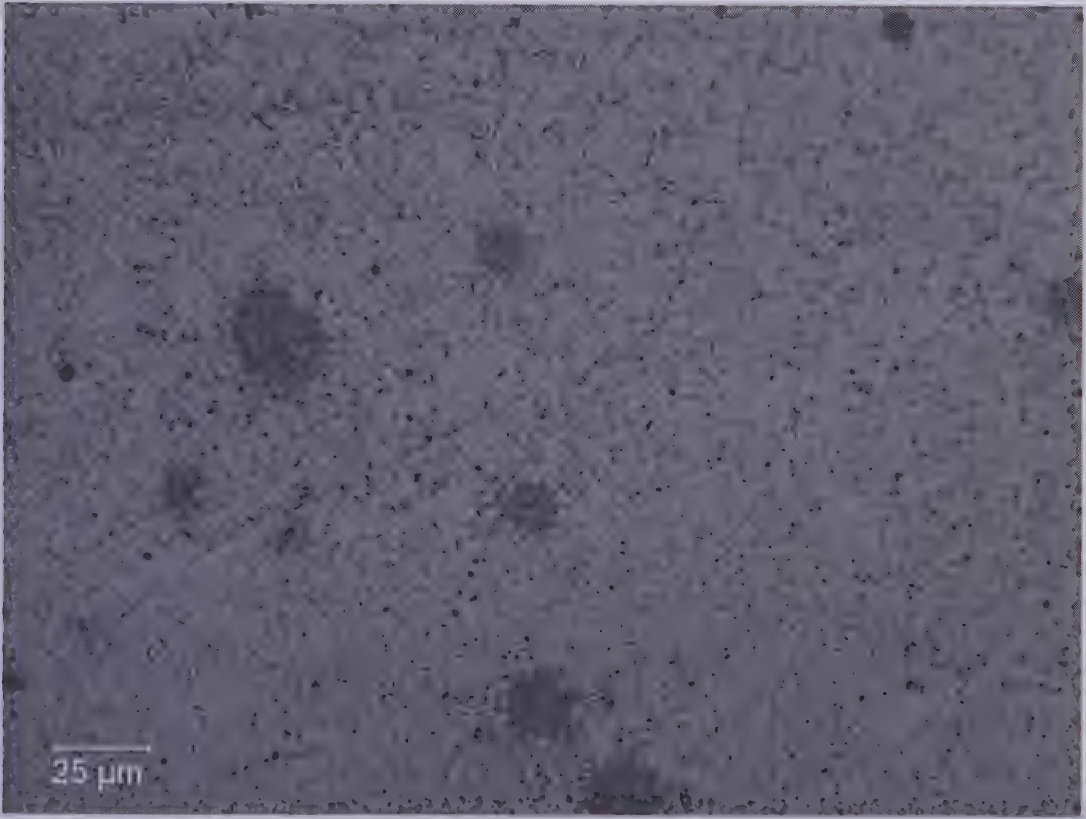

Figure D16: Specimen 10, Weld Metal Reheat Zone, Picral Etch, 400x Magnification

APPENDIX E

Hardness Testing

Heat Input	Untempered	Reheat zone	Fusion line	1mm from fusion line
1.00 kJ/mm	220	211	248	235
1.49 kJ/mm	222	217	241	210
2.03 kJ/mm	242	227	245	218
2.03 kJ/mm*	225	193	204	203

* No maximum interpass temperature was observed

The base material had an average hardness of 181 HV10

Table E1: Hardness testing of samples 5-10 – Vickers test, 10 Kg load

APPENDIX F

Heat Affected Zone Microstructures

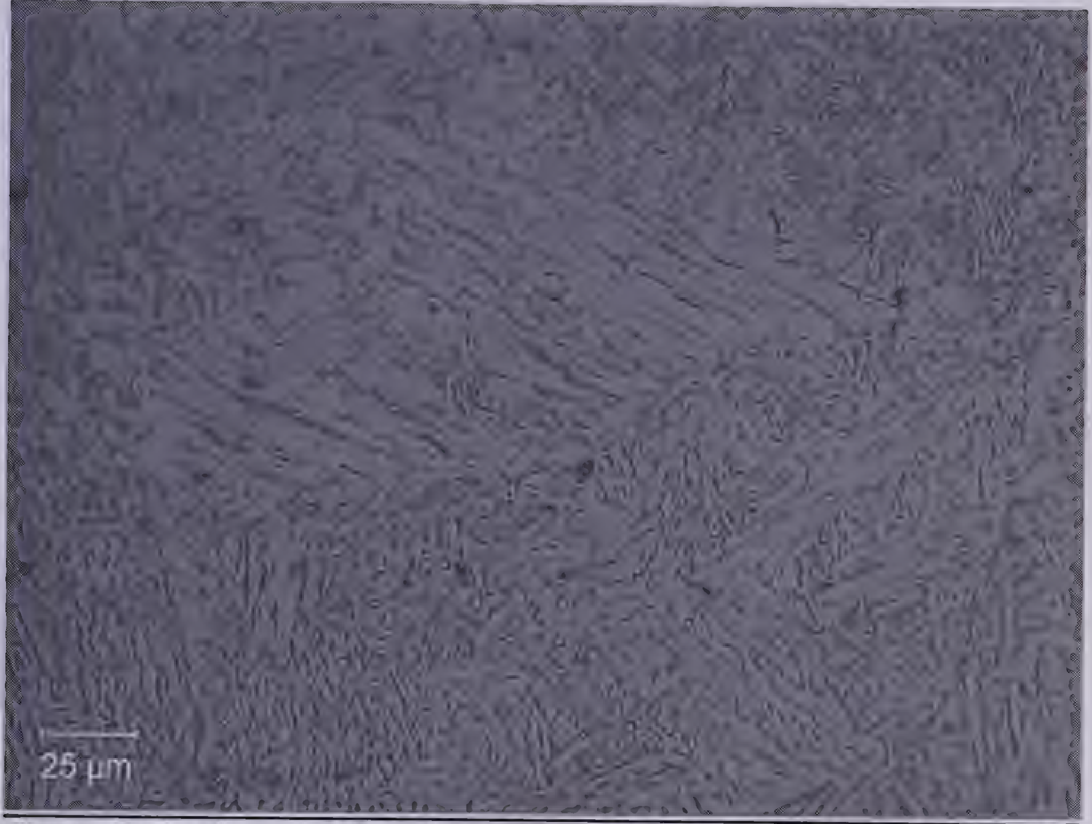

Figure F1: Specimen 5, HAZ Microstructure, 2% Nital Etch, 400X Magnification

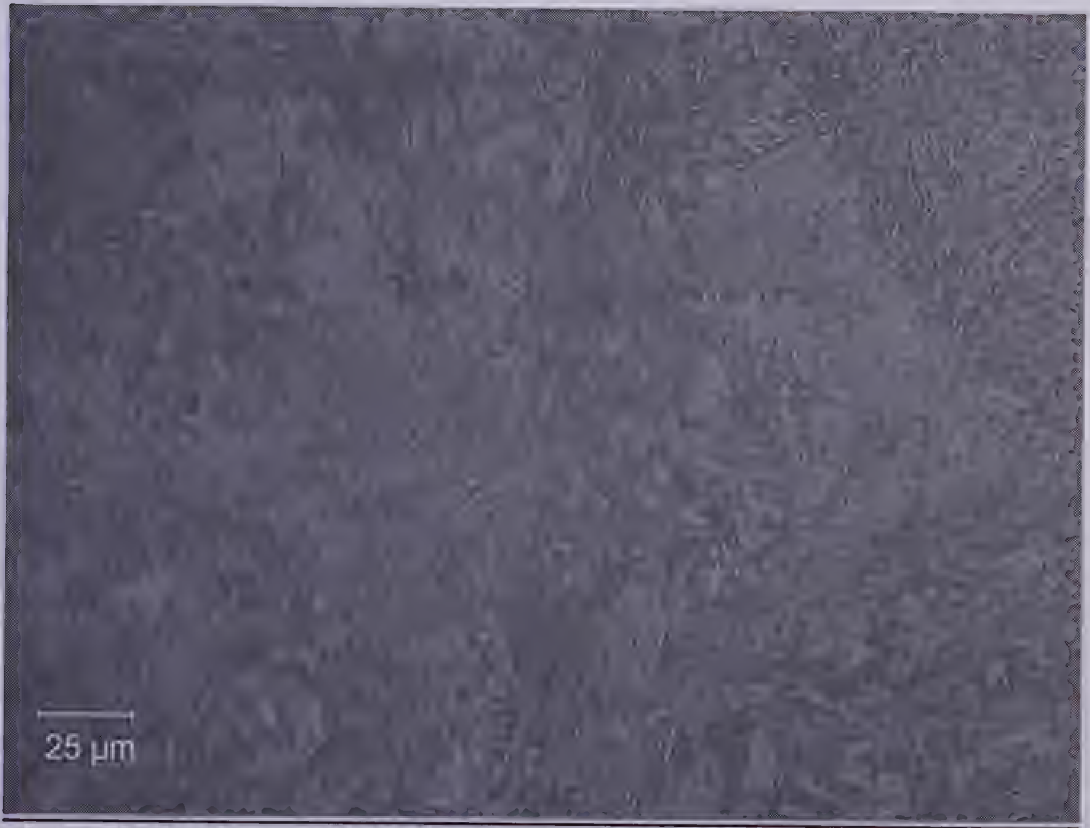

Figure F2: Specimen 6, HAZ Microstructure, 2% Nital Etch, 400X Magnification

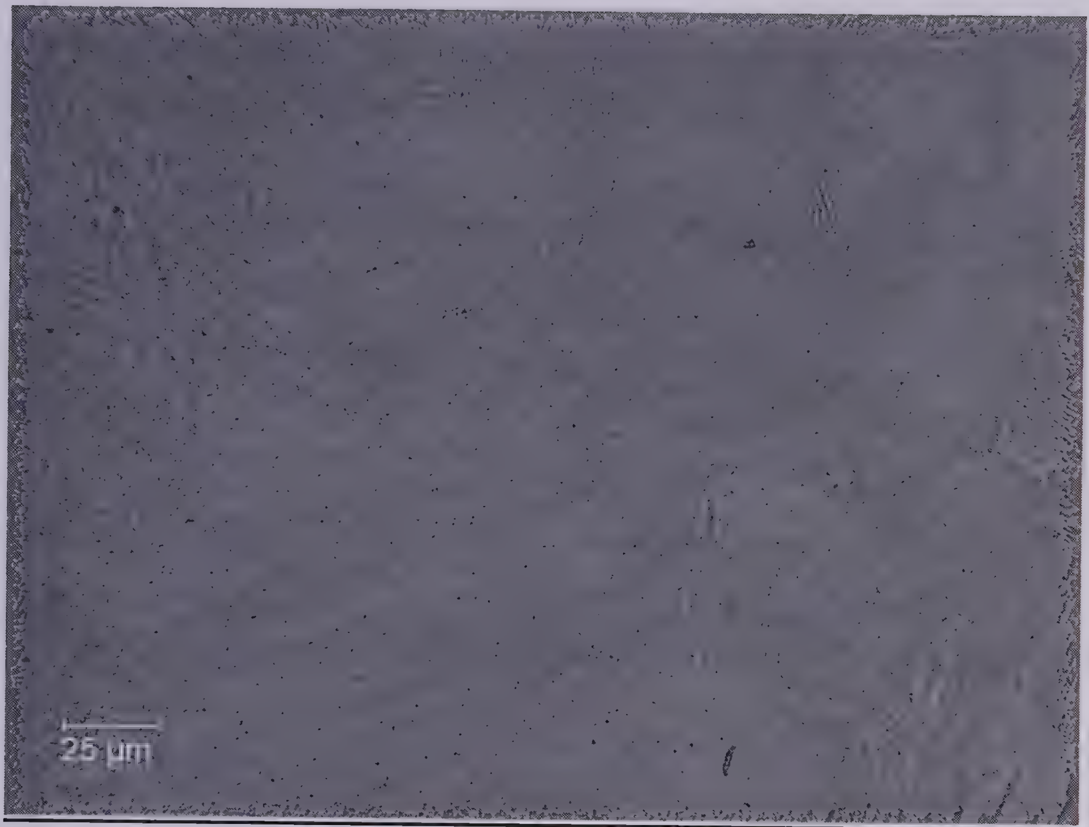

Figure F3: Specimen 7, HAZ Microstructure, 2% Nital Etch, 400X Magnification

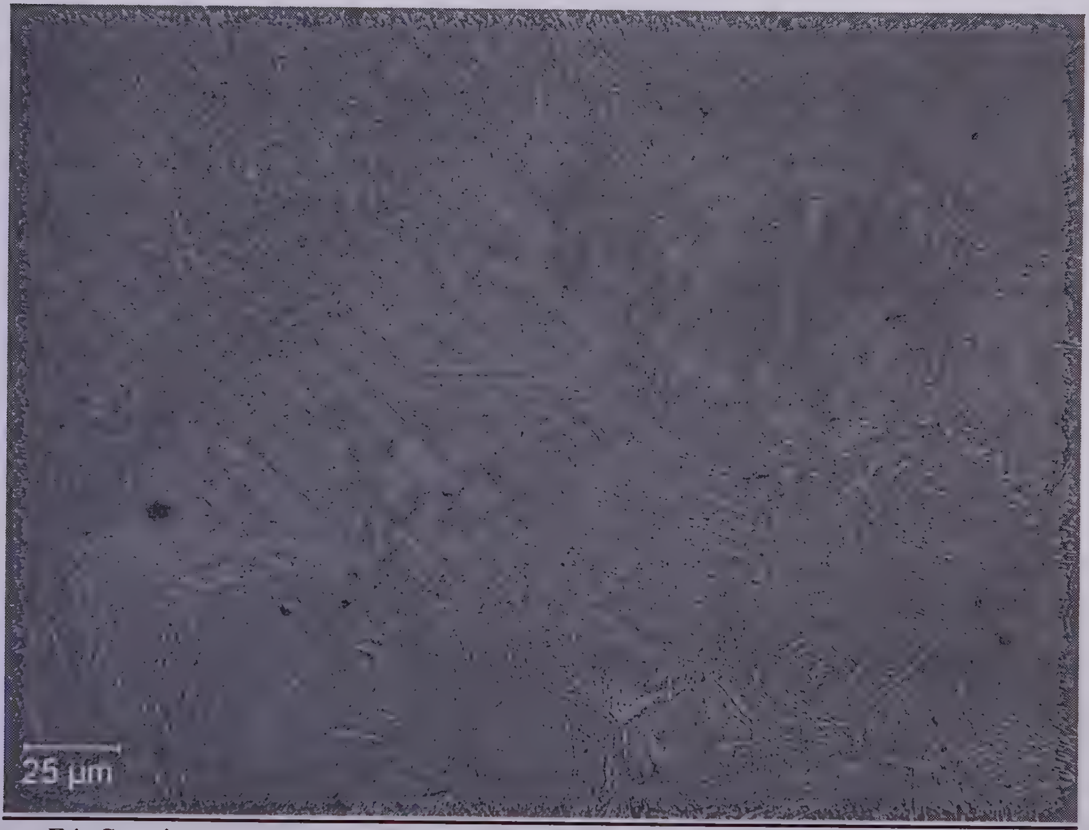

Figure F4: Specimen 10, HAZ Microstructure, 2% Nital Etch, 400X Magnification